International Journal of Heat and Fluid Flow 80 (2019) 108483

Contents lists available at ScienceDirect

International Journal of Heat and Fluid Flow

journal homepage: www.elsevier.com/locate/ijhff

Fluid dynamics of a bifurcation

Kaustav Pradhan*, Abhijit Guha

Mechanical Engineering Department, Indian Institute of Technology Kharagpur, Kharagpur, 721302, India

ARTICLE INFO

Keywords:
Bifurcation
Computational fluid dynamics
Pressure loss
Secondary flow

ABSTRACT

The objectives of the present paper are to accurately determine the modifications to a three-dimensional flow field caused by a bifurcation module, to study the downstream evolution of the generated flow field, and to enhance understanding by establishing the individual and combined roles of five factors (viz. curvature of flow path, flow division at the bifurcation ridge, possible change in flow area from mother to daughter branches, complex shape changes in the bifurcation and inertia of the flow) in giving rise to such a flow field in the bifurcation module. The effects of the aforementioned five factors on the loss production in a bifurcation module and on the potential of further loss in downstream units are also studied, and new correlations are developed. The detailed analysis is systematized here by establishing two novel methods of construction of a bifurcation, viz. "co-joining of two bent pipes" and "splitter in a pipe", and by formally deriving the equivalence condition for the flow in a bifurcation and its constituent elements. Through this systematization an attempt is made to understand comprehensively the complexity of the fluid dynamics occurring in a single bifurcation, which is often masked in the usual studies of flow in large bifurcating networks. Several bifurcation geometries are studied, and about 500 separate three-dimensional computations are performed to achieve a degree of generalization. Use of fine grid (with up to 20 million computational elements in some simulations), double-precision arithmetic and stringent convergence criteria (10^{-8} for each scaled residual) ensures high accuracy of the computed solutions. Both primary and secondary flow fields are investigated. Flow path curvature is responsible for the development of Dean-type secondary motion while flow division at the bifurcation ridge generates secondary motion opposite to that induced by curvature. An increase of flow area from inlet to outlet results in an increase of asymmetry in cross-sectional velocity distribution. Although the loss across a bifurcation may sometimes be smaller than that across its constituent elements, it is shown here through the introduction of two parameters that a greater potential for incurring losses in a following straight section is generated in the bifurcation.

1. Introduction

Fluid motion in branching networks has been the subject of extensive research since such networks are often encountered in biological systems (Pedley, 1977) and are increasingly being contemplated for engineering applications (Murray et al., 1997). As an example, the development of targeted drug delivery techniques requires the knowledge of particle transport in the human bronchial tree. This in turn depends on the fluid flow field. A good account of the flow of fluid and particles in the human respiratory tract is given by Guha (2008). Such branching networks (like the human bronchial tree) are usually dichotomous in nature, i.e. one branch (the mother) divides to give two new branches (the daughters). The junction region where the three branches meet is referred to as the bifurcation module (Fig. 1) and the geometry of that region is complex. Fig. 1 shows how the shape and area of the cross-section changes within a bifurcation module. Due to such complex changes in geometry, analytical determination of the fluid dynamic features of a bifurcation module is difficult, unless some simplifying assumptions are introduced.

In two recent publications (Guha et al., 2016; Guha and Pradhan, 2017), the flow in three-dimensional branching networks comprising six generations (involving 63 branches and 31 bifurcation modules) is comprehensively analyzed, specifying and systematizing the complex primary flow field, and quantifying the generation and evolution of secondary motion. Guha et al. (2016) discusses the primary flow field in three-dimensional planar and non-planar branching networks constructed by connecting branches of successive generations through bifurcation modules, with emphasis on how flow asymmetry is generated and propagated in a geometrically symmetric network. Guha and Pradhan (2017) documents the generation and evolution of

* Corresponding author.
E-mail address: kaustav.pradhan@mech.iitkgp.ac.in (K. Pradhan).

https://doi.org/10.1016/j.ijheatfluidflow.2019.108483
Received 26 April 2019; Received in revised form 9 August 2019; Accepted 21 September 2019

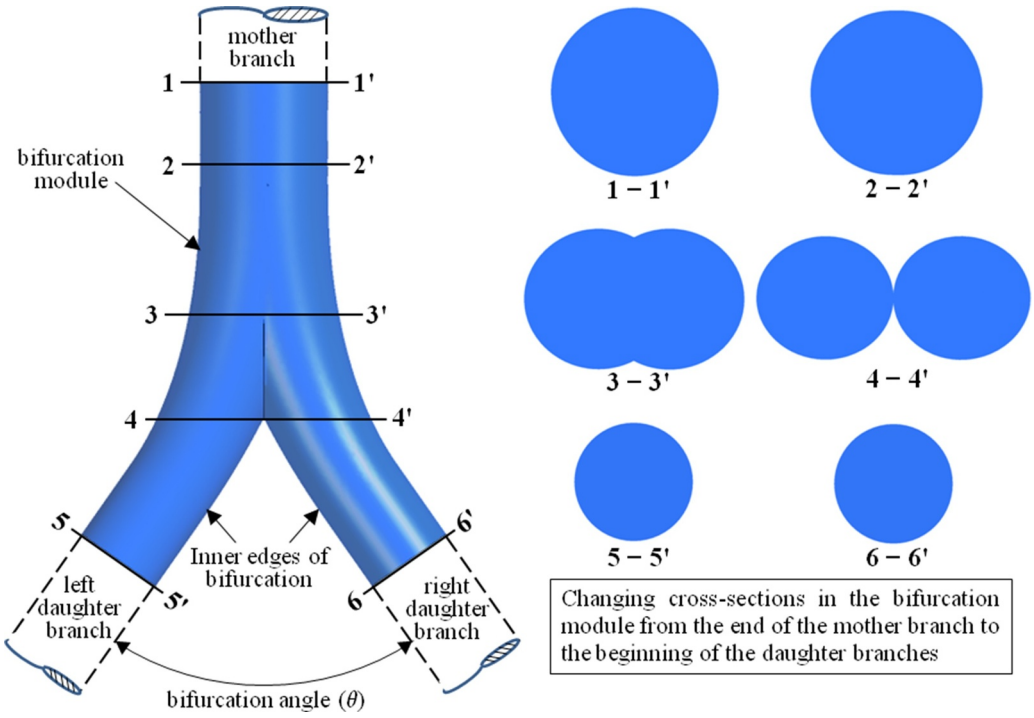

Fig. 1. Schematic of a typical bifurcation module showing the changes in the cross-section that occur as the mother branch divides into two daughter branches.

secondary motion including Dean and anti-Dean type vortical structures, with the introduction of new quantifying parameters that show the increase of secondary motion intensity in the bifurcations and the decrease of the same in the straight sections. Wells et al. (2017) performed numerical simulations to determine the viscous resistance in a network (consisting of 7 branches and 3 bifurcation modules) representing a simplified model of the human bronchial tree. The flow in three-generation branching networks has been the subject of a number of studies (Wilquem and Degrez, 1997; Comer et al., 2001; Liu et al., 2002; Longest and Vinchurkar, 2007). The fluid dynamic aspects of flow in four generations have been investigated by some researchers (Zhang et al., 2001; Fresconi and Prasad, 2007). Nowak et al. (2003) and Kleinstreuer and Zhang (2009) developed modular approaches to study the fluid flow and particle deposition in major portions of a model bronchial tree. There are recent studies (Luo and Liu, 2008; Pourmehran et al., 2016; Banko et al., 2015) which use the geometry of the bronchial tree obtained from CT-scan images. Although the geometry then becomes realistic, the details of the fluid flow field would apply to specific individuals, and these studies, in general, do not delve into either a description of the details of the complex flow field or any physical explanation. Most of the studies, which are aimed at documenting the fluid dynamic features, thus use generalized geometric models. While the references mentioned so far consider steady flow conditions, the periodically unsteady motion in a branching network has also been considered in some recent papers (Das et al., 2018; Bauer et al., 2017; Koullapis et al., 2016; Pradhan and Guha, 2019). Among other things, Pradhan and Guha (2019) describes how the symmetry of the solution with respect to both space and time - found in the oscillating, fully-developed flow in a pipe - are destroyed in the unsteady effects that occur in the oscillating flow in a branching network.

Most of the intriguing fluid dynamic features observed in the flow in branching networks may be attributed to the bifurcation modules (Fig. 1) joining the branches. Although the modifications in the primary and secondary flow field due to a bifurcation module are inherently present in the overall fluid dynamics of a branching network, the detailed role of a single bifurcation is often masked in such studies. However, a detailed understanding of the flow in this important building block would go a long way in comprehending the overall complex flow field in the network. It is in this context that the particular route is taken in this paper to focus attention on what happens in a single bifurcation module rather than on the aggregated effect in a branching network.

A search of the literature on studies of flow in isolated bifurcations shows that experiments were performed to measure the velocity field in symmetric bifurcations (Schroter and Sudlow, 1969; Chang and El Masry, 1982), and models of pressure drop in branching systems were proposed (Pedley et al., 1970a,b, 1971) based on such measurements. In a series of papers, Smith (1976, 1970, 1977a,b) analyzed the flow in a branching tube. Yung et al. (1990) numerically analyzed the steady flow in a bifurcation. The experimental papers did not provide the precise geometries that were used in the experiments while the analytical and numerical studies assumed simple 'Y' type bifurcations with sharp corners. Hence, the correspondence between these experiments and theoretical results can be studied only qualitatively. Zhao and Lieber (1994a,b), for the first time, performed detailed experiments to study the primary and secondary flow field in a single bifurcation with smoothed corners and precisely defined geometric parameters. Zhao et al. (1997) performed numerical simulations for the same geometry as used in their experiments, and demonstrated excellent agreement of the computational and experimental (Zhao and Lieber 1994a) results. The flow in a circular pipe at a high Reynolds number with a splitter plate placed along a diameter was studied by Blyth and Mestel (1999). Tadjfar and Smith (2004) performed direct numerical simulations (DNS) on a single bifurcation (where a mother tube of circular cross section divides into daughters of semi-circular cross section). An attempt was made to develop expressions for the loss coefficient for a bifurcation as a function of various geometrical parameters by Kang et al. (2011). Recently, Stylianou et al. (2016) performed direct numerical simulation (DNS) of inspiratory and expiratory flow in a particular human airway bifurcation model.

The main aim of the present study is to understand thoroughly the flow physics associated with the fluid motion in a bifurcation module by invoking the power of computational fluid dynamics (CFD). When

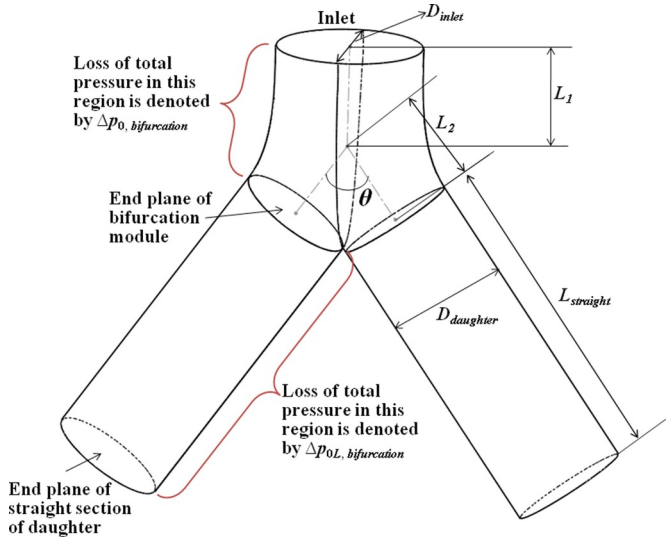

Fig. 2. Schematic of a typical bifurcation "flow unit" comprising a bifurcation module and its two daughter branches.

flow passes through a bifurcation, it changes direction, resulting in the development of secondary currents, and may even separate in some cases depending on the changes in cross-sectional shape and area along the flow path. One uniqueness of the present study is that it does not simply determine the final solution in a complex geometry by the application of CFD as a black-box tool, instead it seeks to attribute the final solution to more elemental aspects of the specified problem thereby enhancing understanding. With this objective in mind, we have identified that the flow in a bifurcation is primarily governed by five factors, viz. flow division at the bifurcation ridge, flow path curvature in the bifurcation module, possible change in cross-sectional area from mother to daughter branches, complex shape changes in the bifurcation module and inertia of the flow. Here, we aim to establish the roles of each of these factors by studying the flow in different geometries (each incorporating some of the factors while eliminating others). Both primary and secondary flow fields are investigated thoroughly and related to mechanisms of loss production.

Several bifurcation geometries are studied, and about 500 separate three-dimensional computations are performed to achieve a degree of generalization. Use of fine grid (with up to 20 million computational elements in some simulations), double-precision arithmetic and stringent convergence criteria ($10^{-8}$for each scaled residual) ensures high accuracy of the computed solutions. The results section is divided into several sub-sections to streamline the discussion. Sections 5.1 and 5.2 deal with the effects of various geometrical factors on the flow modifications that take place in a bifurcation module. The effects of various inlet velocity profiles are elaborated in Section 5.3. Section 5.4 describes how the flow field evolves in the daughter branches (that are located downstream of the bifurcation module under study). Finally, Section 5.5 reflects on the loss in pressure and its relation with the fluid dynamic features described in the previous sections.

The detailed analysis is systematized here by establishing two methods of construction of a bifurcation by applying a series of geometrical transformations or operations to its constituent elements, viz. "co-joining of two bent pipes" and "splitter in a pipe", and by formally deriving the equivalence condition for the flow in a bifurcation and its constituent elements. Through this systematization an attempt is made to understand comprehensively the complexity of the fluid dynamics occurring in a single bifurcation, which is often masked in the usual studies of the flow in a large bifurcating network. The "splitter in a pipe" method allows one to study the effects of flow division in isolation, and the "co-joining of two bent pipes" method allows one to study the effects of flow curvature in isolation. The two methods are complementary to each other and cater for various combinations of the five factors mentioned above. Not only the loss is determined here across a bifurcation module, that is directly determinable experimentally or computationally, but the power of CFD is utilized to develop new methods of quantifying the potential for loss generation in subsequent units that follow the bifurcation module under study. The study provides fundamental physical insight into the mechanisms of loss production and proposes correlations for loss that can be used in practice either in engineering or biological applications.

2. Details of geometry

The fluid dynamics in a branching geometry (i.e. where a mother branch branches/bifurcates into two daughter branches) is primarily governed by the following geometrical factors, viz. flow division at a bifurcation, flow path curvature in the bifurcation module, possible change of cross-sectional area from mother to daughter branches, and complex shape changes in the bifurcation module. The present study considers symmetric bifurcations with rigid walls and a sharp carina (Comer et al., 2001), the cross-sections in the straight sections of the mother and daughter branches being circular. SolidWorks (2010) is used to build the three-dimensional models for various geometries that allow the determination of the contribution of the above-mentioned factors in establishing the flow field in a bifurcation.

2.1. Geometrical parameters for a typical bifurcation

The general features of a bifurcation module have already been described in Fig. 1. In this section, we define the geometric parameters which govern the flow characteristics in a bifurcation. In any branching network, the bifurcation module will be followed by the cylindrical sections representing the daughter branches (Fig. 1). Fig. 2 shows a typical "flow unit" comprising a bifurcation module along with the two daughter branches. The geometrical parameters which affect the flow field in the bifurcation module are the total flow length ($L_1 + L_2$) from the inlet of the bifurcation module to the outlet (which is the start-plane of the daughter branch), the area ratio A.R. ($\equiv A_{outlet}/A_{inlet}$), and the bifurcation angle (θ).Except otherwise stated, the value of ($L_{straight}/D_{daughter}$) which represents the total straight length of the daughter branches is kept at 3.5 (a commonly observed value in many natural/biological systems (Pedley et al., 1970a,b, 1971)).

2.2. Methods of construction of bifurcation from constituent elements

The bifurcation flow unit described in Fig. 2 may be thought to be constructed in various ways by applying a series of geometrical transformations or operations to its constituent elements. Fig. 3 depicts one such method which is named the "co-joining of two bent pipes" wherein two similar bent pipes of a given area ratio A.R. ($\equiv A_{outlet}/A_{inlet}$) are merged together to form a bifurcation of the same A.R. (A_{outlet} for the bifurcation is the sum of the outlet areas of the two daughter branches) as that of the pipes. The above-mentioned method essentially comprises three major steps: (i) the bending of the straight pipe through an angle equal to half of the bifurcation angle (θ) of the bifurcation that is to be constructed, (ii) changing of the cross-sectional area in the bend depending on the A.R. of the bifurcation to be constructed, and (iii) the co-joining of two such bent pipes along the outer radius wall. It should be noted that the second step is eliminated in case of the construction of a bifurcation of A.R. = 1 from a straight pipe of A.R. = 1. During the process of co-joining of the two bent pipes, the total cross-sectional areas at the inlet and outlet are conserved, i.e., the cross-sectional area at the inlet of the bifurcation is equal to the sum of that at the inlets of the two component pipes while the cross-sectional area at the outlet of one of the daughters of the bifurcation is equal to that at the outlet of the constituent bent pipe. It is worth mentioning here that due to the manner of co-joining of the bent pipes to form the bifurcation (Fig. 3),

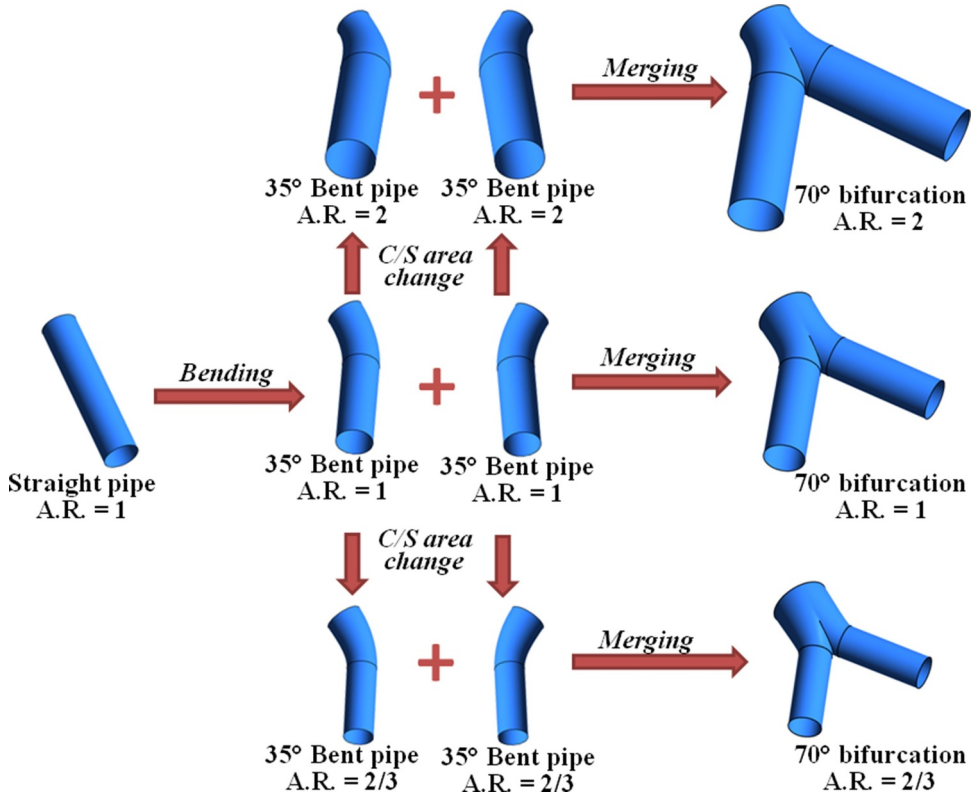

Fig. 3. Schematic showing the construction of bifurcations from a straight pipe by the method of "co-joining of two bent pipes".

the inner edges of the bifurcation (Fig. 1) correspond to the outer edges in its constituent bent pipes and the outer edges of the bifurcation correspond to the inner edges in the constituent bent pipes.

Fig. 4 shows another method of forming a bifurcation which is named here as the "splitter in a pipe" method. Here, a straight pipe of A.R. equal to that of the desired bifurcation is taken as the starting point. Then, a splitter plate of negligible thickness (we have used a splitter plate of thickness of 1% of the straight pipe diameter) as compared to the diameter of the straight pipe is placed along the middle so as to mimic the flow division caused by the bifurcation ridge. This configuration of a straight pipe with a splitter plate may be viewed as a bifurcation with zero bifurcation angle and semi-circular daughters. It may be transformed into a bifurcation with a finite bifurcation angle and circular daughters in either of the following ways: (i) bending of the two parts on the two sides of the splitter plate by an angle equal to half of the bifurcation angle to obtain a bifurcation with semi-circular daughter branches, followed by a shape change of the cross-section to give circular daughter branches, or (ii) change of the cross-sectional shape on the two sides of the splitter plate from semi-circular to circular (this change of shape, while maintaining A.R. = 1, requires bending by a small angle which has been found to introduce negligible curvature effects; in our case this angle is 5°) followed by the bending of the two parts in opposite directions to form the two daughter branches. It should be noted that during this process of transformation of a straight pipe to a bifurcation, the value of A.R. is maintained constant.

We cite below three examples to amplify the utility of the "splitter in a pipe" methodology: (i) a comparison of the flow in a straight pipe and that in the straight pipe with a splitter plate establishes the isolated effects of flow division, (ii) a comparison of the flow in a straight pipe and that in a 70° bifurcation with semi-circular daughters establishes the combined effects of two geometric factors viz. curvature in the presence of flow division, (iii) a comparison of the flow in a straight pipe and that in a 70° bifurcation with circular daughters establishes the combined effects of flow division, curvature and change of shape of the cross-section in the daughters from semi-circular to circular. On the other hand, if one wants to determine the isolated effect of curvature alone, then the "splitter in a pipe" methodology is not adequate because the effect of flow division is inherently present in this method. The "co-joining of two bent pipes" method can establish the effects of curvature alone. Similarly, an intermediate geometry in the "co-joining of two bent pipes" method can establish the combined effects of curvature and change in flow area without flow division. Herein lies the utility of the two methods. Thus, the two methods are not arbitrarily adopted, but are carefully developed with a well-defined objective. The two methods play complementary roles in enhancing physical understanding and cater for various combinations of the five factors governing the flow in a bifurcation. Although it may be possible to design other methods of constructing bifurcations, it is found that these two methods provide sufficient intermediate geometries during the transformation of a pipe into a bifurcation for analyzing the individual and combined roles of the geometrical factors viz. curvature in the flow path, flow division, possible change in flow area from mother to daughter branches, and complex shape changes in the bifurcation.

It should be clearly understood that although we have illustrated the case of bifurcation angle (θ) equal to70° in Figs. 3 and 4, the methods described are generic and may be used to develop bifurcation flow units of any practically possible bifurcation angle (θ). It is to be noted that all geometries shown in Figs. 3 and 4 correspond to the "flow units" (i.e. the bifurcation module or its equivalent bent pipe is followed by a straight section).

2.3. Equivalent flow in a bifurcation and its constituent elements

Computations of the flow in a bifurcation and its constituent elements at the same mass flow rate led to greatly differing values of the losses across the bifurcation and its constituent elements, which could not be attributed to the factors governing the flow in a bifurcation. The concept of an "equivalent flow condition" is thus developed here for the

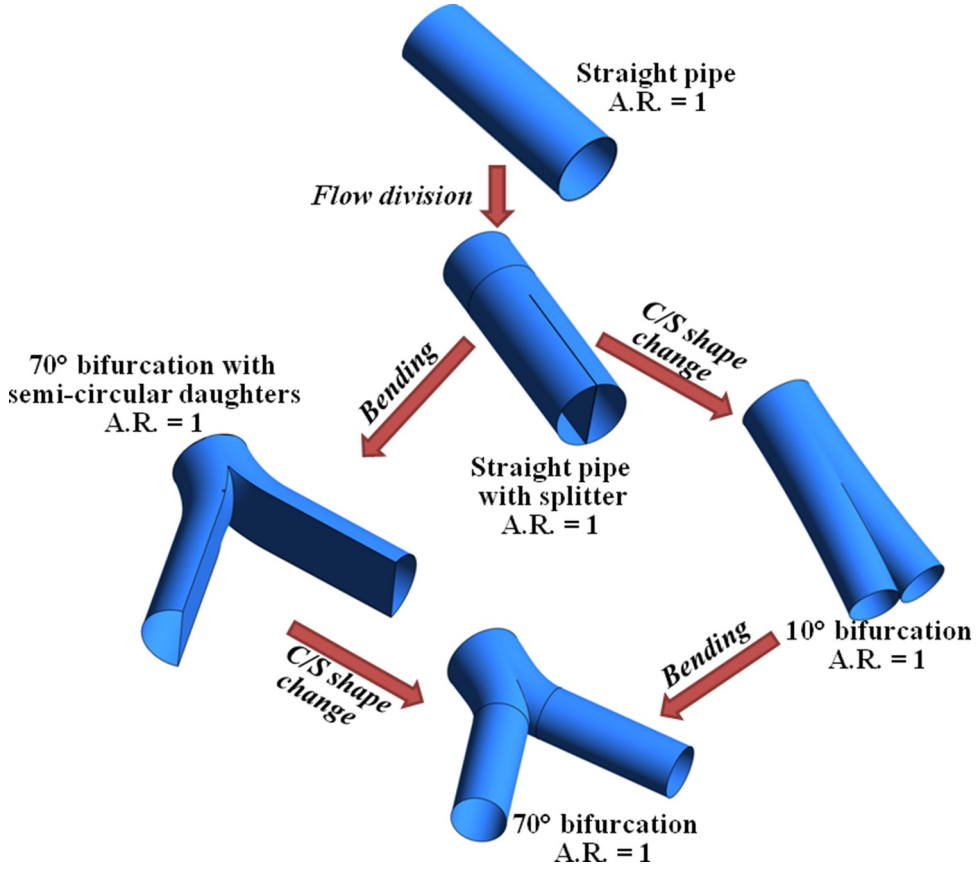

Fig. 4. Schematic showing the construction of a bifurcation from a straight pipe by placing a splitter plate in the pipe.

flow in a bifurcation and its constituent elements. Suppose, the final bifurcation has an inlet area A_{inlet} and outlet area A_{outlet} in each daughter. The flow rate at the inlet of the bifurcation is Q_{inlet} and that at the outlet of each daughter is $Q_{inlet}/2$. The area ratio A.R. is defined as the ratio of the total outlet area and the total inlet area. For the bifurcation, therefore, A. R.$=2A_{outlet}/A_{inlet}$. For geometric equivalence, the A.R. of the constituent pipes in either "co-joining of two bent pipes" or "splitter in a pipe" method is kept the same as that in the bifurcation. Having obtained geometric equivalence, the "equivalent flow condition" requires that the total flow rate at the inlet (or outlet) of the final bifurcation is equal to the total flow rate at the inlet (or outlet) of the constituent pipes.

In the "co-joining of two bent pipes" method (Fig. 3), one starts with two constituent pipes which are joined; each pipe, therefore, has an inlet area $A_{inlet}/2$ and outlet area A_{outlet}. The inlet diameter of each constituent pipe is thus $1/\sqrt{2}$ times the inlet diameter of the bifurcation. (This is illustrated in Fig. 5 which shows the dimensions for a bifurcation and its constituent elements.) For maintaining "equivalent flow condition", the prescribed flow rate at the inlet of each constituent pipe is $Q_{inlet}/2$; which also represents the flow rate at the outlet of each constituent pipe. The total flow rate at the inlet (or the outlet) of the two constituent pipes is thus Q_{inlet}, the same as that for the resulting bifurcation.

In the "splitter in a pipe" method (Fig. 4), one starts with one constituent pipe which is split into two halves. There is thus a direct correspondence between the constituent pipe with a splitter and the resulting bifurcation. For geometric equivalence, the inlet area of the constituent pipe is therefore kept as the same as that of the bifurcation, i.e. A_{inlet}. For maintaining "equivalent flow condition", the prescribed flow rate at the inlet of the constituent pipe isQ_{inlet}, the same as that of the resulting bifurcation.

Table 1 gives the geometric details of three bifurcations formed by the "co-joining of two bent pipes" method and their equivalent/constituent bent and straight pipes that are used to determine the role of individual geometric factors in setting up the flow field. The diameter of the mother branch in the bifurcation is kept fixed at 10 mm and all other diameters (in the bifurcations and pipes) are chosen accordingly so as to attain desired value of the area ratio A.R. As shown in Fig. 5, the inlet diameter of the constituent pipe is $1/\sqrt{2}$ times the inlet diameter of the bifurcation. The values of A.R. have been chosen so as to cover all three possibilities; increasing area of flow (A.R. = 2) from inlet to outlet, uniform area of flow (A.R. = 1) and decreasing area of flow (A.R. = 2/3) from inlet to outlet of the flow unit.

3. Mathematical formulation

The governing equations for steady, incompressible, laminar flow of a Newtonian fluid are given as follows:

$$\nabla \cdot \vec{v} = 0 \tag{1}$$

$$\rho(\vec{v}.\ \nabla)\vec{v} = -\nabla p + \mu\nabla^2\vec{v} \tag{2}$$

In the above equations, $\vec{v}$ represents the fluid velocity vector, p is the static pressure, ρand μ are respectively the density and dynamic viscosity of the fluid. In the simulations reported here, air is taken as the working fluid with ρ and μ equal to 1.225 kg/m^3 and 1.7894×10^{-5} Pa − s respectively.

A uniform velocity distribution is assumed at the inlet of the flow unit (pipe or bifurcation) unless otherwise mentioned in a specific comparative study. The no-slip and no-penetration conditions are applied on the branch walls and the outlets are modeled using a pressure boundary condition. Although the flow in geometries with curved sections is found to be governed by the Dean number (Horlock, 1956; Berger et al., 1983), the changes in local curvature within the bifurcation module makes the determination of the local Dean number difficult. Hence, in previous studies (Guha et al., 2016; Guha and

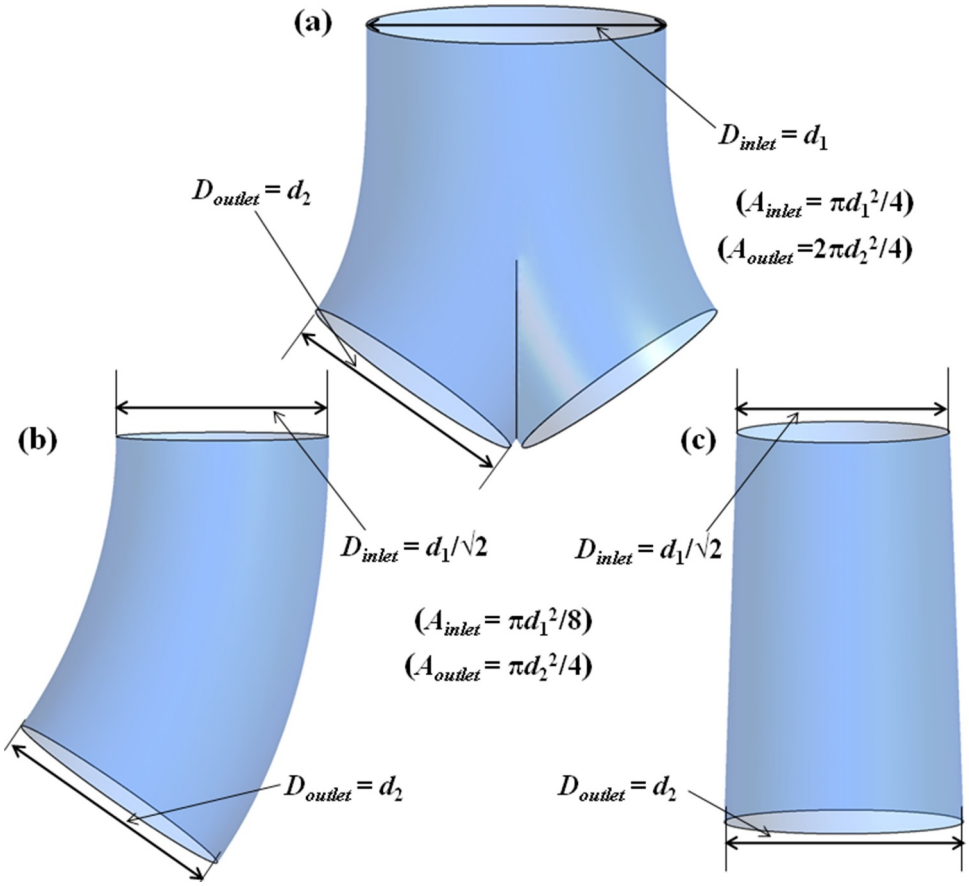

Fig. 5. Schematic of a bifurcation module and its constituent elements. (a) bifurcation module, (b) constituent bent pipe, (c) constituent straight pipe.

Pradhan, 2017) on branching networks, the parametric variation of the inlet Reynolds number ($\mathrm{Re} \equiv \rho\, V_{inlet} D_{inlet}/\mu$) has been considered; D_{inlet} and V_{inlet} are respectively the diameter and flow velocity at the inlet to the bifurcation module. However, it is found that when the equivalence flow condition is established, the inlet Reynolds number for the bifurcation is different from that in its constituent element. On the other hand, the inlet velocity is the same in both flow units for the equivalence flow condition. In the present study, since we intermittently revert back to the flow in straight and bent pipes so as to establish the effect of geometric factors on the flow, we consider the parametric variation of the inlet velocity (V_{inlet}) instead of the inlet Reynolds number.

3.1. Calculation of pressure drop

It is interesting to make an estimation of the pressure loss incurred when the flow in a branching network passes through a flow unit. The decrease in static pressure across the unit is defined as,

$$\Delta p = p_{in} - p_{out} \tag{3}$$

where p_{in} and p_{out} are the area-weighted average static pressures at the inlet and outlet sections respectively. Similarly, the decrease in total pressure across the unit is defined as,

$$\Delta p_0 = p_{0,in} - p_{0,out} \tag{4}$$

where $p_{0,in}$ and $p_{0,out}$ are the mass-flow-averaged (same as volume-flow-averaged for incompressible flow where ρ is a constant) total pressures at the inlet and outlet sections respectively. In the calculation of the loss of total pressure across a bifurcation ($\Delta p_{0,\ bifurcation}$), the outlet pressure is calculated by taking the mass-flow average over both the outlets. Eq. (4) can be written in an expanded form as follows:

Table 1
Geometric details of the bifurcations and their equivalent pipes used in the present study to determine the individual role of geometric factors.

Geometry	D_{inlet} (mm)	D_{outlet} (mm)	Area Ratio (A.R.)	Bifurcation/Bend Angle
Bifurcation	10	10	2	70°
Equivalent Bent Pipe	$10/\sqrt{2}$	10	2	35°
Equivalent Straight Pipe	$10/\sqrt{2}$	10	2	–
Bifurcation	10	$10/\sqrt{2}$	1	70°
Equivalent Bent Pipe	$10/\sqrt{2}$	$10/\sqrt{2}$	1	35°
Equivalent Straight Pipe	$10/\sqrt{2}$	$10/\sqrt{2}$	1	–
Bifurcation	10	$10/\sqrt{3}$	2/3	70°
Equivalent Bent Pipe	$10/\sqrt{2}$	$10/\sqrt{3}$	2/3	35°
Equivalent Straight Pipe	$10/\sqrt{2}$	$10/\sqrt{3}$	2/3	–

$$\left(\frac{\iint(p+\frac{1}{2}\rho|\vec{v}|^2)\rho\vec{v}\cdot dA}{\iint\rho\vec{v}\cdot dA}\right)_{in}=\left(\frac{\iint(p+\frac{1}{2}\rho|\vec{v}|^2)\rho\vec{v}\cdot dA}{\iint\rho\vec{v}\cdot dA}\right)_{out}+\Delta p_0 \quad (5)$$

In Eq. (5), dA represents an elemental area at a particular cross-section. The term in the left hand side of Eq. (5) is the mass-flow-averaged total pressure at the inlet section and the first term on the right hand side of Eq. (5) is the mass-flow-averaged total pressure at the outlet section. In the absence of heat transfer, shaft work transfer and gravitational effects, the application of incompressible energy equation for non-uniform flow shows that the drop in mass-flow-averaged total pressure Δp_0 is connected to the effects of viscous dissipation.

4. Numerical method

The three-dimensional models considered are built in SolidWorks (2010), the meshing is done using ANSYS Mesh Modeller (ANSYS 15.0, 2014), and numerical simulations are performed using ANSYS Fluent. We have simulated the flow in each of the bifurcations and their constituent elements for 7 different inlet velocities, thus requiring a large number of simulation runs.

4.1. Grid generation

Here an unstructured mesh comprising tetrahedral elements is generated for the geometries using ANSYS Meshing. Inflation layers (boundary layer-type meshing) are used adjacent to the branch walls to accurately capture the velocity and pressure gradients near the wall. It is important to ensure that the inflation layers in the two halves of the cross-section do not overlap (as it overlaps, for example, in Nowak et al. (2003)) in the bifurcation region (Fig. 1). Here, the bifurcation geometry is constructed in such a manner that the overlapping of the inflation layers is avoided.

4.2. Details of simulations

The pressure-based solver available in FLUENT is used for solving the three-dimensional governing equations. The advection terms are discretized using the second order upwind scheme so as to reduce the numerical diffusion associated with an unstructured mesh (Barth and Jespersen, 1989). A segregated implicit (Mei and Guha, 2005) solver is used which uses a time-marching technique (Guha and Young, 1991; Guha, 1994) to reach the steady state. The SIMPLE algorithm is employed in coupling the velocity and pressure. A convergence criterion is set at 10^{-8} for all the results reported here. The 'Velocity Inlet' feature is used to specify a flow velocity at the inlet to the flow unit. At the outlets, the 'Pressure Outlet' feature is used to specify a static pressure there. In the present work, the gage pressures at the outlet sections are set to zero. It is to be realized that it is the change in static pressure across the flow unit (Δp) that the CFD simulations determine, and for incompressible flow, Δp may be assumed to be independent of the absolute value of the static pressure specified at the outlet (Guha et al., 2016; Guha and Pradhan, 2017). Thus, once the value of Δp is determined from the simulations, the static pressure at any location within the flow unit may be determined if the actual value of static pressure is specified somewhere in the unit.

4.3. Grid independence study

Grid independence of the solution has been determined for all geometries considered, following the method developed by Roache (1997) for unstructured grids. In this method, a relative error ε_i is calculated using the following expression:

$$\varepsilon_i=\left|\frac{\eta_{i,\,coarse}-\eta_{i,\,fine}}{\eta_{i,\,fine}}\right| \quad (6)$$

where η represents a flow variable. Here, the magnitude of velocity is considered for calculating the value of ε_i. The root-mean-square value of this relative error (ε_{rms}) is a direct measure of grid convergence when $r_{grid}=(N_{fine}/N_{coarse})^{1/3}=2$. Since it is difficult to achieve true grid halving for unstructured three-dimensional mesh, Roache (1997) introduced a grid convergence index GCI for $r_{grid}<2$. GCI for the refined grid is defined as follows:

$$GCI_{fine}=F_s\frac{\varepsilon_{rms}}{r_{grid}^q-1}. \quad (7)$$

Here, q is the order of discretization of all terms in space, F_s is a factor of safety whose value is set to 3, so that the value of GCI becomes equal to ε_{rms} for $r_{grid}=2$ and $q=2$ (the value of q being 2 for second order discretization in space). Here, the value of ε_{rms} is calculated from a large number of points (400 points are used along two mutually perpendicular diameters at the end of the left daughter branch). In the course of our present study, we found that for $GCI\le 5\%$, the changes in the flow field are negligible for further grid refinements.

Celik et al. (2008) proposed a formulation for calculating an apparent order (q) of discretization from values of ε_{rms} and r_{grid}. They stated that a grid independent solution is indicated by an agreement of the apparent order with the formal order of the used scheme. Accordingly, here we have used their iterative method to find the value of q .

The details of the grids with results of the grid independence test for the bifurcation with A.R. = 1 (Table 1) are tabulated in Table 2. We find that the value of GCI for the medium mesh is 17.1%, that for the fine mesh is 7.4% and that for the very fine mesh is 5%. Hence the change in GCI between fine and very fine mesh is small. The value of q is calculated to be 1.95 for the two sets of three meshes (coarse, medium and fine; and medium, fine and very fine). The “fine” mesh thus provides sufficiently accurate results. However, the “very fine” mesh is used for all subsequent simulations pertaining to this bifurcation for increased precision. Similar grid independence studies have been performed for the other bifurcations as well; those details have not been included in this paper for brevity.

We have taken great care in ensuring the accuracy of the values of loss of total pressure reported here. The values of loss of total pressure (Δp_0) across a bifurcation and its constituent elements obtained by using successively finer meshes are tabulated in Table 3. It is observed that the results uniformly converge as the mesh is progressively refined, and the values obtained by using the 'fine' and 'very fine' mesh are identical up to five decimal places. We have reported values of loss of total pressure up to four decimal places in the Tables included in this paper. Moreover, we have used the very fine mesh for all results reported here. This gives confidence in the results and the conclusions drawn from them.

4.4. Validation of present method

Zhao and Lieber (1994a) measured steady inhalation airflow through a symmetric single bifurcation with mother branch diameter of 3.81cm, mother to daughter diameter ratio of $\sqrt{2}$ (which corresponds to A.R. =1) and bifurcation angle of 70°. Laser doppler anemometry (LDA) measurements of the velocity in the meridional plane (defined as the plane containing the centrelines of the mother and daughter braches by Guha et al. (2016)) and transverse planes (normal to the meridional

Table 2
Details of the grid independence test for a 70° bifurcation flow unit of A.R. =1 (D_{inlet} = 10 mm,D_{outlet} = 10/$\sqrt{2}$ mm) performed at Re = 1000 (V_{inlet} = 1.46 m/s).

Number of elements in mesh	r_{grid}	ε_{rms}	GCI
104,187 (coarse) - 255,723 (medium)	1.35	0.047	0.171
255,723 (medium) - 807,552 (fine)	1.47	0.029	0.074
807,552 (fine) - 2547,816 (very fine)	1.47	0.019	0.050

Table 3
The mass-flow-averaged drop of total pressure across different geometries involved in the construction of a 70° bifurcation (D_{inlet} = 10 mm) of A.R. = 1 from its constituent elements (using the "co-joining of two bent pipes" method) for V_{inlet} = 1.46 m/s.

Mesh	Number of elements	$\Delta p_{0,\ straight}$	$\Delta p_{0,\ bent}$	$\Delta p_{0,\ bifurcation}$
Coarse	104,187	0.524419	0.527891	0.445601
Medium	255,723	0.524501	0.528097	0.445856
Fine	807,552	0.524532	0.528135	0.445911
Very fine	2547,816	0.524534	0.528138	0.445914

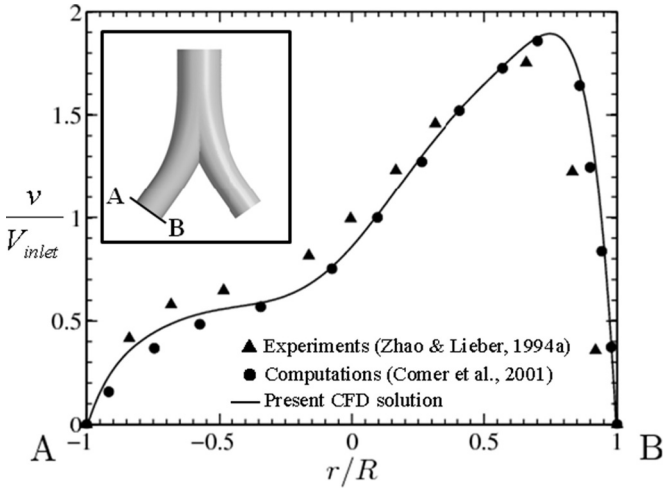

Fig. 6. Profile of the axial velocity along the diameter lying on the meridional plane at the outlet of the left daughter branch (line A-B) for Re = 1036.

plane) were carried out at three different values of inlet Reynolds number (i.e., Re= 518, 1036 and 2089) and 17 different locations in the complete geometry. The geometry of Zhao and Lieber (1994a) is reproduced here, and the velocity profile is compared at a specified location for Re = 1036 (Fig. 6). In the same figure, the numerical results of Comer et al. (2001) are also included. All velocities shown in Fig. 6 are presented along a meridional diameter in the left daughter branch at the junction of the bifurcation module and the cylindrical section of the daughter branch. Since the numerical results are symmetric about the centreline of the mother branch, the velocities in the right daughter (which are exact mirror images of that in the left daughter) are not shown here. It is found that the present CFD results agree well with the experimental measurements (Zhao and Lieber, 1994a) at Re = 1036 (Fig. 6) as well as at other values of the inlet Reynolds number (not shown here); at places the present CFD results compare better with the experiments than the computational results of Comer et al. (2001).

5. Results and discussion

The flow physics in a bifurcation (comprising a mother branch dividing into two daughter branches) may be explained by attributing the fluid dynamics to the following important geometrical factors - flow division at the bifurcation ridge, curvature of the flow path, possible changes in cross-sectional area from mother to daughter branches and complex change in cross-sectional shape in the bifurcation module. Here, we have tried to assess the separate contributions of each of these effects and their final culmination into the overall features of the flow field in a bifurcation by considering the flow in different geometries. All results reported in this paper pertain to the flow of air through the considered flow unit.

5.1. Determination of the role of geometrical factors in a bifurcation constructed by "co-joining of two bent pipes"

Since this method of construction of a bifurcation, demonstrated in Fig. 3, involves bending of the straight pipe through an angle equal to half of the bifurcation angle (θ), followed by the changing of the cross-sectional area in the bend depending on the A.R. of the bifurcation to be constructed, and finally, the joining of two such bent pipes along their

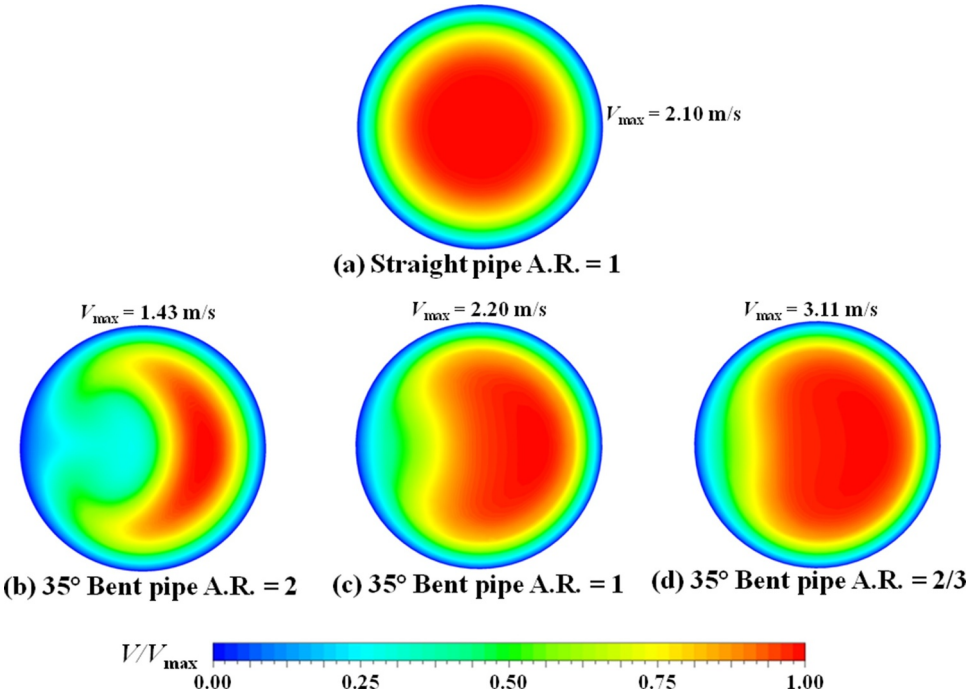

Fig. 7. Contours of velocity magnitude at the outlet section of a straight pipe flow unit and at the outlets of three bent pipe units of different A.R. values (Table 1) for an inlet velocity V_{inlet} = 1.46 m/s. [The particular inlet flow rate is chosen since it corresponds to Re = 1000 in the bifurcations constructed from these bent pipes (Table 1)].

outer radius walls, we try to determine the effects of bending (or flow path curvature), change of cross-sectional area and flow division in sequence.

5.1.1. Effects of flow path curvature and cross-sectional area change

Fig. 7 shows the effect of bending of a straight pipe flow unit followed by changes in the cross-sectional area of flow from inlet to outlet (i.e. A.R. ≠ 1) on the cross-sectional velocity distribution. A comparison of Figs. 7(a) and 7(c) shows that the introduction of flow path curvature (in the absence of cross-sectional area changes) leads to a shift of the maximum of velocity towards the outer edge of bent pipe and generates a crescent shaped zone of high velocity in the cross-section. Development of this crescent shaped zone may be attributed to the Dean-type secondary circulation typically occurring in curved pipes which essentially pushes faster moving fluid towards the outer edge of bent pipe along the horizontal centreline (Guha and Pradhan, 2017). Another effect of the crescent shaped velocity contours is the development of "M-shaped" velocity profiles (comprising two maxima) along the vertical diameter in the diagram.

The effects of changes in the cross-sectional area (for the same bend angle) on the velocity distribution may be ascertained by comparing the velocity contours at the outlet of a bent pipe flow unit with A.R. = 1 (Fig. 7c) with those at the outlets of bent pipe units with A.R. ≠ 1 (Fig. 7b and d). Fig. 7(b) shows a pronounced crescent shaped high velocity zone in the cross-section for A.R. = 2 while the shape of that zone gradually flattens as A.R. decreases to 1 (Fig. 7c) and 2/3 (Fig.7d). This indicates that while the curvature of the flow path tends to introduce asymmetry in the cross-sectional velocity distribution, a decrease of A.R. (i.e. a decrease of the outlet diameter when the inlet diameter is kept unchanged) tends to reduce such asymmetries. Such a trend may be attributed to the increase in the average velocity at the outlet section (indicated by a larger zone of high velocity) due to a reduction of the flow area at the outlet section with decreasing values of A.R..

5.1.2. Effect of flow division at bifurcation ridge

In this section, we determine the effects of flow division in a bifurcation by simultaneously studying the velocity distribution in a bent pipe flow unit and that in a bifurcation flow unit constructed by co-joining two such bent pipe units (Fig. 3). The geometric symmetry of such a bifurcation ensures that the flow field in the two daughters are mirror images of one another. Hence, in all following discussions, the velocity contours in the left daughter branch of the bifurcation are shown. The contours of velocity magnitude are plotted at the end-plane (plane A) of the module and at the end-plane (plane B) of the straight section following it, for both bent pipe units and bifurcation units to illustrate the fluid dynamic effects of the bifurcation ridge (which is absent in the bent pipe unit). The secondary velocity vectors are also superposed on the contours to show how flow division affects the secondary flow.

Fig. 8 shows the velocity contours and secondary flow pattern at specified cross-sections in a 35° bent pipe flow unit with A.R. = 1 and in a bifurcation constructed by co-joining two such units. The velocity contours at plane A for the bent pipe are characterized by maximum velocity near its outer edge (which corresponds to the inner edge of the bifurcation) while the maximum of the velocity is shifted in the opposite direction for the bifurcation. While the shift of maximum velocity in the bent pipe occurs due to the effects of curvature, the opposite trend in the bifurcation occurs due to the combined effects of uniform inlet flow and the development of a low velocity region in proximity to the bifurcation ridge. The secondary flow at plane A in both the bent pipe and the bifurcation shows two counter-rotating Dean vortices (Guha and Pradhan, 2017) in the two halves of the cross-section with secondary fluid motion towards the inner edge of bifurcation in the center and back towards the outer edge of bifurcation along the top and bottom walls. The velocity contours and the secondary flow patterns at plane B in Fig. 8 for the bent pipe (A.R. = 1) are found to be similar to that for the bifurcation (A.R. = 1); the velocity contours are characterized by a crescent shaped region of high velocity skewed towards the inner edge of bifurcation and the secondary flow pattern shows typical Dean-type circulation. Thus, the straight sections following the bent pipe and the bifurcation module alter the flow field in such a way that the differences observed at plane A are attenuated considerably. This also shows that the differences at plane A occur primarily due to the effects of flow division in the bifurcation which gradually decay with distance from the bifurcation ridge.

Fig. 9 shows the velocity contours and secondary flow pattern at planes A and B in a 70° bifurcation of A.R. = 2 and that in its constituent bent pipe. At plane A, the bent pipe shows a maximum velocity near its outer radius (Berger et al., 1983) whereas the maximum velocity occurs near the center of the cross-section in the bifurcation. This may be attributed to the effects of the bifurcation ridge which creates a low velocity region in its vicinity and hence pushes the maximum velocity away from the inner edge. The secondary flow at plane A in both the bent pipe and the bifurcation is characterized by typical Dean-type circulation. As was observed in Fig. 8, the velocity contours as well as the secondary pattern at plane B in Fig. 9 for the bent pipe and the bifurcation are similar owing to the decaying flow division effects with distance downstream of the bifurcation ridge. A comparison of the velocity contours in Figs. 8 and 9 shows that the increase of A.R. from 1 to 2 results in an increase in the non-uniformity in the velocity distribution at a cross-section with the development of a low velocity region towards the outer edge and a crescent-shaped high velocity zone near the inner edge. The enhanced non-uniformity in the cross-sectional velocity distribution may be attributed to the diffuser-like (Massey and Ward-Smith, 1998) flow path in the geometry with A.R. = 2.

Fig. 10 shows the contours of velocity and secondary flow pattern in a 70° bifurcation of A.R. = 2/3 and its constituent bent pipe. Owing to the reduction of cross-sectional area from the inlet to plane A, the average velocity at plane A (for bent pipe and bifurcation) is considerably greater than that at the inlet. Moreover, the asymmetry in the velocity distribution at plane A for the bent pipe is found to be small as compared to that found in Figs. 8 and 9). However, the velocity contours at plane A for the bifurcation show a maximum near the outer edge mainly due to the generation of the low velocity region around the bifurcation ridge. Although some asymmetry is developed in the velocity distribution at plane B for the bent pipe as well as the bifurcation (with A.R. = 2/3), it is significantly smaller than that observed in Figs. 8 and 9. The secondary flow patterns in Fig. 10 appear similar in the bent pipe and the bifurcation at both planes A and B (with characteristic Dean-type circulation).

The following general conclusions may be drawn from the observations made in Figs. 7–10. (i) The curvature of the flow path is responsible for the development of skewed velocity distributions and Dean-type secondary motion at a cross-section. (ii) An increase in the value of A.R. results in an increase in the non-uniformity in the velocity distribution at a cross-section downstream of the curved section. (iii) The bifurcation ridge creates a low velocity region in its vicinity, thus leading to a shift of the velocity maximum towards the outer edges in the daughter branches (this tendency is opposite to that caused by the flow curvature effects). (iv) The straight sections following the bent pipe or the bifurcation module in a flow unit (Pedley et al., 1971) have the general tendency to attenuate the differences caused by the bifurcation ridge, and restore similarities in the flow field in the two flow units.

5.1.3. Consideration of all geometrical factors together

Fig. 11 shows secondary velocity contours at the outlet sections of the geometries (plane B in Figs. 8–10) involved in the transformation of a straight pipe into a bifurcation by the method of "co-joining of two bent pipes" (Fig. 3). The significantly greater magnitudes of secondary velocity in the bent pipe (A.R. = 1) and the bifurcation (A.R. = 1) as

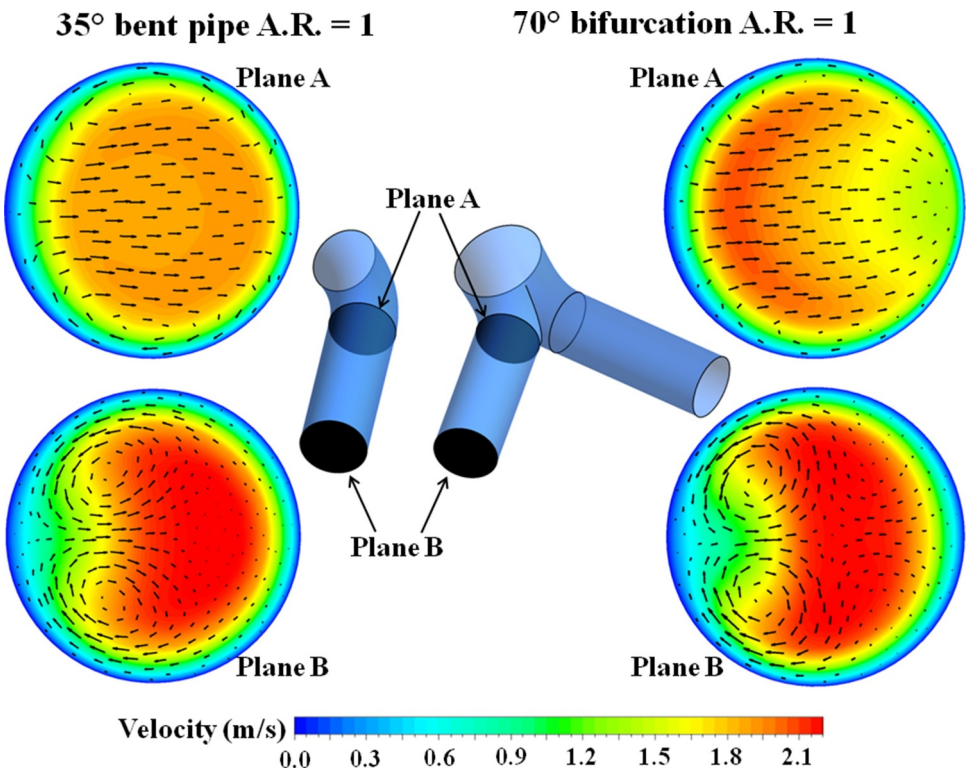

Fig. 8. Vectors of secondary velocity superposed on velocity magnitude contours at the beginning and end of the straight section following a bent pipe and a bifurcation module for V_{inlet} = 1.46 m/s and A.R. =1.

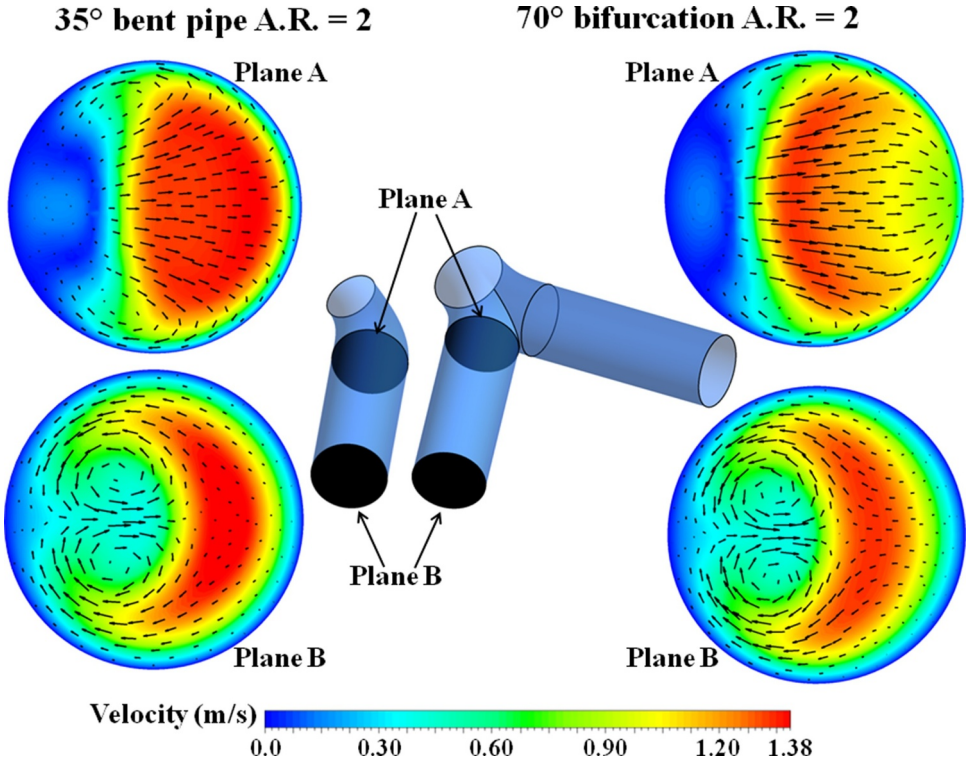

Fig. 9. Vectors of secondary velocity superposed on velocity magnitude contours at the beginning and end of the straight section following a bent pipe and a bifurcation module for V_{inlet} = 1.46 m/s and A.R.=2.

compared to that in the straight pipe (A.R. = 1) is primarily due to the effects of curvature of flow path. Fig. 11 also shows that the secondary velocity contours in bent pipes and bifurcations are qualitatively similar, the features thus being attributable to the effects of curvature alone. The secondary velocity contour at the end-plane in a bent pipe or bifurcation flow unit is characterized by two counter-rotating vortices with maximum velocity $|\vec{v}_S|_{\max}$ occurring near the top and bottom walls. The small isolated (blue) regions of low $|\vec{v}_S|$ occurring

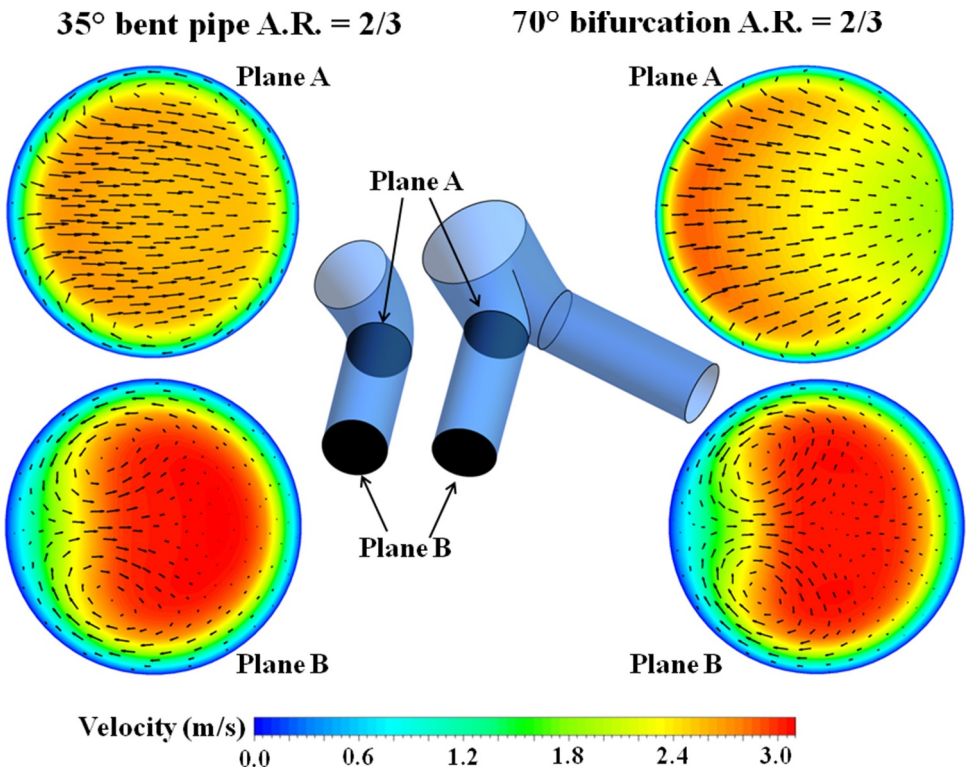

Fig. 10. Vectors of secondary velocity superposed on velocity magnitude contours at the beginning and end of the straight section following a bent pipe and a bifurcation module for V_{inlet} = 1.46 m/s and A.R. =2/3.

symmetrically in the upper and lower half of the cross-sections correspond to the core region of the vortices (Guha and Pradhan, 2017).

The average secondary velocity at the outlet of a bifurcation flow unit is found to increase as A.R. decreases from 2 to 2/3. However, Fig. 11 does not show any definite trend in the average secondary velocity at the end-plane of the straight section following the bent pipe. Calculations show that for a given value of A.R., the average secondary velocity at the end-plane of the straight section following the

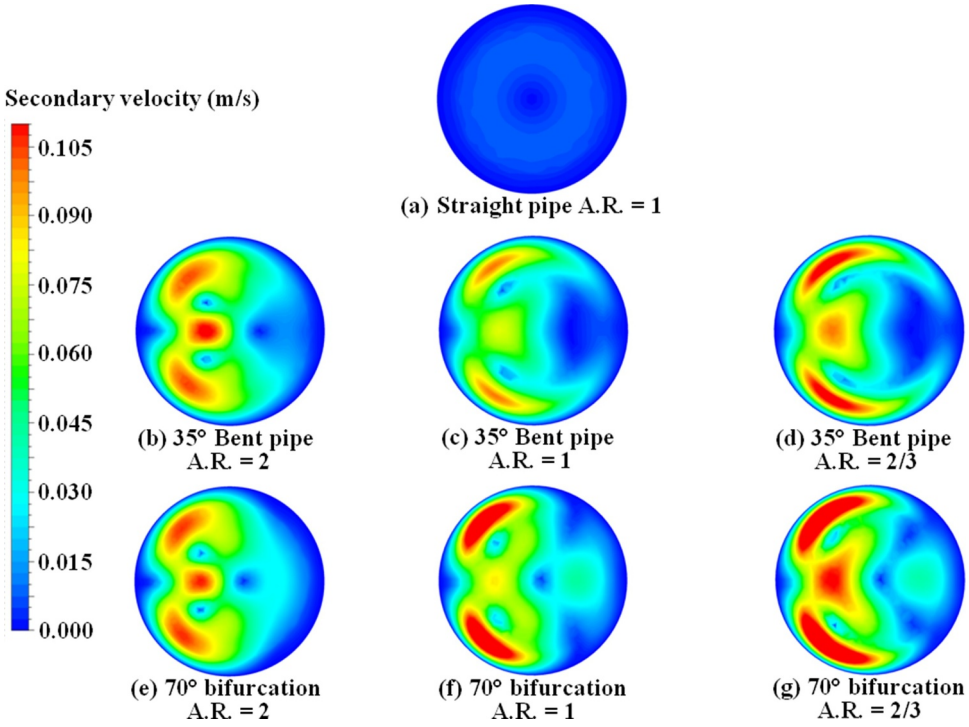

Fig. 11. Contours of secondary velocity magnitude at the outlet section of a straight pipe ofA.R. =1, at the outlet of bent pipes of different A.R. values, and at the exit-plane of the left daughter branch in the bifurcations constructed from those bent pipes for V_{inlet} = 1.46 m/s. (Outlet section refers to the end-plane of the "flow unit" for pipes and bifurcations).

bifurcation is greater than that at the corresponding plane following the bent pipe (for the "equivalent flow condition"). It is interesting to note that for the chosen bifurcation/bend angle in Fig. 11, a reduction of total flow area from inlet to outlet (A.R. < 1) results in an increase of average secondary flow velocity in both pipes and bifurcations whereas an expansion of total flow area from inlet to outlet (A.R. > 1) results in an increase of average secondary velocity in the bent pipe but a decrease of the same in the bifurcation. Such a qualitative difference between bent pipes and bifurcations for A.R. > 1 may be attributed to the tendency of the bifurcation ridge to cause secondary motion opposite to that caused by the flow curvature effects. For A.R. < 1, the greater flow velocities result in the curvature effects dominating over the effects of flow division, thus leading to greater magnitudes of secondary velocities for both bent pipes and bifurcations.

5.1.4. Effect of geometrical factors on the pressure losses

The decrease of total pressure across a pipe or a bifurcation is an important parameter since it indicates the losses incurred by the flow between the inlet and the outlet. In the present study, the decrease of pressure across a given flow module is calculated from Eq. (3). We have shown in Fig. 3 how a bifurcation may be constructed from a straight pipe. Here, in Table 4, we list the decrease of static (Δp) and total (Δp_0) pressure across the different geometries (shown in Fig. 3) with an aim to understand the pressure loss caused by individual factors governing the flow in a bifurcation.

A comparison of the pressure drops across the straight pipe (A.R. = 1) and the 35° bent pipe (A.R. = 1) in Table 4 shows that flow path curvature results in an increase of both Δp and Δp_0 (in the presence or absence of the following straight section). However, the effect of the presence of the bifurcation ridge, that may be ascertained by comparing the values of Δp_0 for the 35° bent pipe (A.R. = 1) and the 70° bifurcation (A.R. = 1), is to cause a decrease ofΔp_0. A contributory factor to this finding may be visualized by the partial removal of the internal wall in the formation of the bifurcation by the co-joining of two bent pipes. While the value of Δp_0 for the bifurcation module (i.e. without the straight sections) is smaller than that for the equivalent bent pipe, usually the opposite happens when straight sections are added to both. The reasons for such an observation are discussed later in Section 5.5.

The effect of changing flow area on the loss of pressure can be ascertained by comparing the pressure drops in the 35° bent pipes of area ratios 1, 2 and 2/3 in Table 4. A change of A.R. from 1 to 2 causes a large decrease in Δp (by about 90%) irrespective of the presence/absence of the straight portion following the curved pipe, and a decrease in Δp_0 by about 25% (again irrespective of the presence/absence of the straight section following the curved section of the pipe). The significant decrease of Δp may be attributed to the pressure recovery associated with increasing cross-sectional area in the bent pipe with A.R. = 2. It was shown in Eq. (5) that Δp_0 represents the losses associated with the flow. It is expected that the losses associated with a diverging bent pipe (A.R. = 2) would be greater than that in a bent pipe of uniform cross-sectional area (A.R. = 1). However, the above statement holds true only if the same flow rate in an equivalent uniform diameter pipe is used for the comparison. (The equivalent diameter is such that the uniform cross-sectional area would be equal to the arithmetic mean of the inlet and outlet areas of the diverging pipe.) On the other hand, a decrease of A.R. from 1 to 2/3 results in a significant increase in Δp (by 74% in the presence of a following straight section and by about 100% in its absence) and an increase in Δp_0 (by 65% in the presence of a following straight section and by about 43% in its absence). This trend may also be attributed to the fact that the flows in the two above-mentioned bent pipes (which have the same inlet cross-sectional area) are not equivalent. Similar observations are made for 70° bifurcation with increasing or decreasing cross-sectional areas from inlet to outlet.

It is interesting to note that for both 35° bent pipes and 70° bifurcations, the static pressure drop Δp is greater than the drop in total pressure when the value of A.R. is 1 or 2/3; however Δp_0 exceeds Δp for the case of A.R. = 2. This may be attributed to the decreasing flow velocities from inlet to outlet in case of A.R. = 2. The negative value of Δp for the bifurcation module (A.R. = 2) followed by straight sections indicates that there occurs a rise of static pressure across the bifurcation flow unit due to the increasing flow area.

Table 4 also shows that the losses (Δp_0) associated with a bent pipe or bifurcation is greater for A.R. = 2/3 than that for A.R. = 2. This is in contradiction to our expectation that an increase of cross-sectional flow area down the module results in greater losses than that for the case of decreasing flow area. The reason for the contradiction may be explained as follows: The usually accepted notion of greater losses in a diverging pipe as compared to a converging pipe (for the same flow rate) is true if the comparison is made between a converging and a diverging pipe whose average cross-sectional areas (i.e. the arithmetic mean of the inlet and outlet areas) are the same. However, this condition is not satisfied by the bent pipes and bifurcations considered here in which the inlet area is kept constant, irrespective of whether A.R. is greater than or less than 1.

5.2. Determination of the role of geometrical factors in a bifurcation constructed by "splitter in a pipe" method

The construction of a bifurcation from a straight pipe by first placing a splitter along a diameter in the pipe and then introducing flow path curvature and cross-sectional shape changes was discussed in Fig. 4. Here, we determine the fluid dynamic changes associated with the above-mentioned transformation for A.R. = 1. Then, we investigate the effect of A.R. on those changes by considering a case where the value of A.R. is equal to 2.

Fig. 12 show the secondary velocity vectors superposed on the contours of velocity magnitude at the outlet section of the different flow units involved in the transformation of a straight pipe of A.R. = 1 to a bifurcation of A.R. = 1. The geometrical changes introduced at each stage have been mentioned over the arrows in the figure. The fluid dynamic effects of flow division is isolated here by considering the flow

Table 4
Decrease of the area-averaged static pressure and mass-flow-averaged total pressure across different flow units involved in the construction of a bifurcation flow unit from its constituent elements (as shown in Fig. 3) for V_{inlet} = 1.46 m/s.

Geometry	Static pressure drop Δp (Pa)		Total pressure drop Δp_0 (Pa)	
	Across module only	Across module followed by straight section	Across module only	Across module followed by straight section
70° bifurcation A.R. = 1	1.2119	1.7175	0.4459	0.9897
35° bent pipe A.R. = 1	1.1213	1.7137	0.5281	0.9930
70° bifurcation A.R. = 2	0.0129	−0.0606	0.2897	0.6259
35° bent pipe A.R. = 2	0.1639	0.0784	0.4061	0.7365
70° bifurcation A.R. = 2/3	3.2025	4.6311	0.5174	1.5641
35° bent pipe A.R. = 2/3	3.3528	4.6967	0.7559	1.6275
Straight pipe A.R. = 1	0.9971	1.6019	0.5245	0.9099

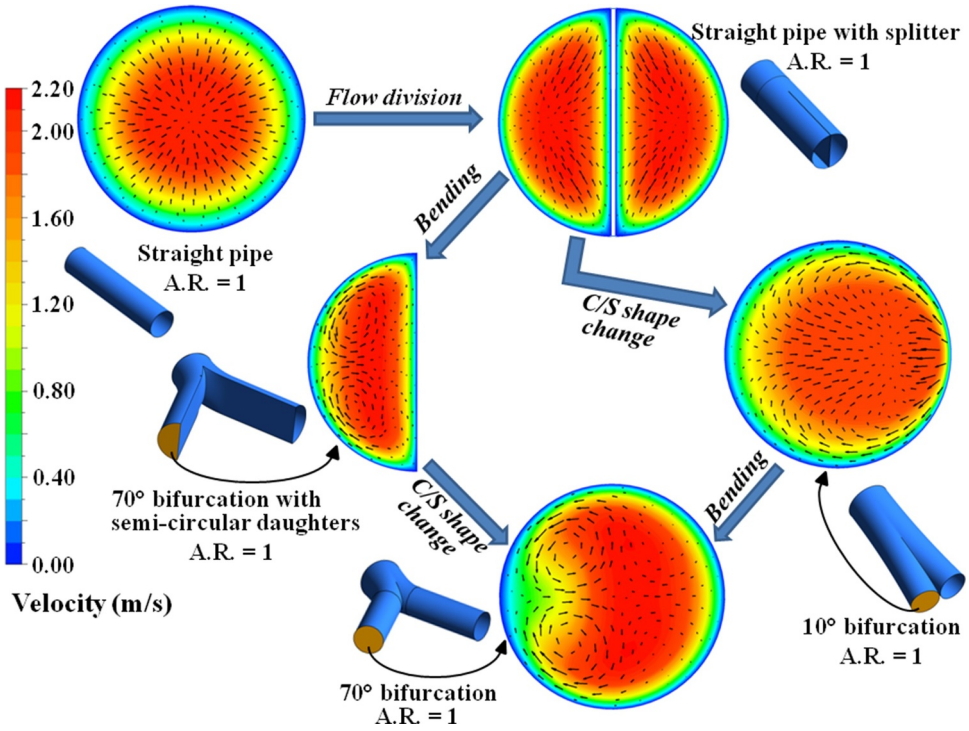

Fig. 12. Vectors of secondary velocity superposed on velocity magnitude contours at the outlet sections of the various geometries involved in the construction of a bifurcation from a straight pipe (as shown in Fig. 4) for V_{inlet} = 1.46 m/s and A.R. =1.

in a straight pipe with a splitter plate in the middle, which may be viewed as a bifurcation with zero bifurcation angle (thus eliminating flow curvature effects) with semi-circular daughters (thus eliminating the effects of change in cross-sectional area and shape). The leading face of the splitter plate represents the bifurcation ridge in the 0° bifurcation.

The contours of primary velocity in the entrance region of a straight pipe (Fig. 12) are characterized by concentric circles with the maximum velocity in the center, and secondary fluid motion directed from the periphery towards the cross-sectional center. Viscous effects are responsible for the transformation of the uniform inlet velocity to the parabolic profile in the fully developed region, and the associated secondary motion which drives fluid from the periphery towards the center. The introduction of the splitter plate divides the flow in the pipe into two separate streams with the formation of two additional boundary layers on the two surfaces of the splitter. The contours of primary velocity are found to follow the shape of the cross-section (concentric semi-circles). Although the average velocity is equal in both cases (due to equality of flow area), the maximum velocity is greater in the pipe with splitter plate due to the additional boundary layers. In each semi-circular daughter, the secondary circulation is similar to that in the straight pipe with movement of fluid from the periphery towards the center of the semi-circle. From the above discussion it is concluded that flow division alone (i.e. in the absence of curvature) results in the development of additional boundary layers along the edges of the divider, and sets up secondary fluid motion directing fluid away from the divider (which represents the inner edges of the bifurcation).

The effect of introducing curvature in the presence of flow division is now ascertained by considering the flow field at the outlet section of the 70° bifurcation (A.R. = 1) with semi-circular daughter branches in Fig. 12. The curvature in the flow path in the bifurcation leads to a change of shape of the velocity contour bands from semi-circles to flattened bean-shaped structures. Typical Dean-type secondary circulation is set up as shown by the secondary flow vectors in the semi-circular daughter branches of the 70° bifurcation.

The effect of changing the shape of the daughter branches from semi-circular to circular, in the presence of curvature and flow division effects, is determined by comparing the velocity field at the outlet section of the left daughter branch in the 70° bifurcation with semi-circular daughters to that at the same location in the 70° bifurcation with circular daughters in Fig. 12. The change of cross-section leads to a change in the shape of the velocity contour bands from bean-shaped structures following the semi-circular cross-sectional shape to crescent-shaped structures. The shift of the velocity maximum towards the inner edge that was also present in the case of semi-circular daughters is found to be more prominent in case of circular daughter branches. There appears to be no significant qualitative change in the secondary flow pattern (Dean-type circulation) in the daughter branches due to the change of cross-sectional shape from semi-circular to circular.

It was shown in Fig. 4 that instead of introducing the curvature in the pipe with splitter plate configuration, the shape on the two sides of the splitter plate may be changed first so as to form a bifurcation of very small bifurcation angle (10° here) with circular daughters, followed by its transformation into a large angle bifurcation by the introduction of flow path curvature. Such a transformation would allow one to determine the effect of cross-sectional shape change in the presence of flow division but in the absence of curvature effects. It is observed in Fig. 12 that the velocity contours at the end-plane of the straight section following the bifurcation module in the 10° bifurcation with circular daughters are different from that found in the straight pipe with splitter plate (i.e. 0° bifurcation with semi-circular daughters). The contour bands in the 10° bifurcation appear as concentric circles (instead of the semi-circles found in the pipe with splitter plate) indicating that the shape of the velocity contours follows the shape of the cross-section. Moreover, the change of shape of the daughters from semi-circular to circular results in a reduction of the non-uniformity of cross-sectional velocity distribution. The change of cross-sectional shape from semi-circular to circular induces secondary fluid motion along the top and bottom edges towards the outer edge in addition to the secondary flow induced by the flow division effects (which drives fluid away from the bifurcation ridge).

A comparison of the velocity field in the daughter branch of the 10°

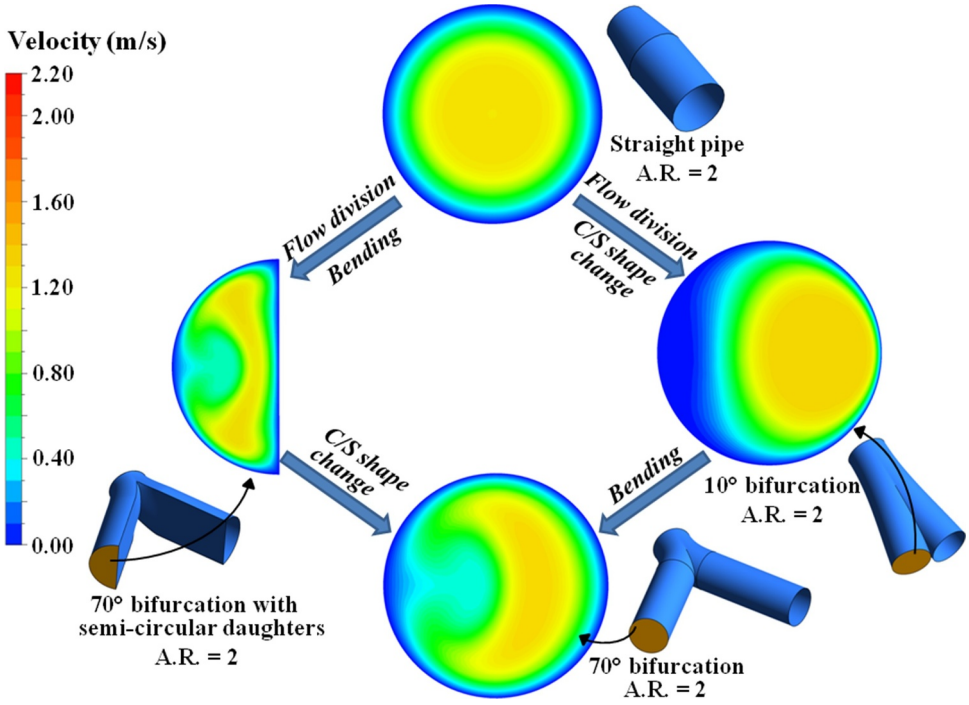

Fig. 13. Contours of velocity magnitude at the outlet sections of the various geometries involved in the construction of a bifurcation from a straight pipe (as shown in Fig. 4) for V_{inlet} = 1.46 m/s and A.R. =2.

bifurcation with that at the same location of the 70° bifurcation (both having circular daughters) establishes the effect of bending of the flow path in the presence of flow division and cross-sectional shape change. Fig. 12 shows that curvature leads to the development of crescent-shaped contour bands and typical Dean-type circulation in the cross-section. Associated with the change of shape of the contour bands is an increase of the maximum velocity in the cross-section and hence an increase in the non-uniformity in the velocity distribution.

Having described the individual effects of successive geometrical changes in the transformation of a straight pipe of A.R. = 1 to a 70° bifurcation of A.R. = 1, we now investigate the effect of the same changes when A.R. is 2 (Fig. 13). Since the secondary flow pattern for this case (A.R. = 2) is qualitatively similar to that shown in Fig. 12 (A.R. = 1), they have not been shown in Fig. 13. For the same inlet flow rate, a comparison of Figs. 12 and 13 reveal that the maximum (and average) velocities in the daughter branches are significantly reduced as A.R. increases from 1 to 2. The contours for A.R. = 2 (Fig. 13) show an enhanced non-uniformity in cross-sectional velocity distribution. The reason for this enhancement may be explained as follows. Due to the symmetry of flow with respect to the bifurcation ridge in a single bifurcation, the flow in one half of the mother branch (i.e. flow in a semi-circular area with the diameter aligned with the trace of the bifurcation ridge) is directed toward one of the daughter branches. For A.R. = 2, the flow along this path not only experiences a change of shape of the flow area (that is also present when A.R. = 1) but also an increase in flow area (similar to that in a diffuser). It is well known (Massey and Ward-Smith, 1998) that diffusers magnify any non-uniformity in the cross-sectional velocity distribution. The development of the low velocity region of large extent in the left daughter branch for the 10° bifurcation is associated with this enhanced non-uniformity due to diffusion.

Fig. 14 shows secondary velocity contours at the same locations as in Fig. 13. A comparison of the secondary velocities at the outlet sections of the straight pipe with splitter plate, at the outlets of the 70° bifurcation flow unit with semi-circular daughters, and at the outlet section of the 10° bifurcation with circular daughter branches shows that both curvature and cross-sectional shape change induce considerable secondary motion (though the nature of the induced circulation in different as explained in the context of Fig. 12). It is found in Fig. 14 that the average secondary velocity at the outlet section of the 10° bifurcation with circular daughter branches is greater than that at the outlet section of the 70° bifurcation flow unit with semi-circular daughters. This may be attributed to the smaller length (such that the total length of flow path remains constant) of the straight section (which attenuates secondary motion (Guha and Pradhan, 2017)) following the bifurcation module in the 10° bifurcation flow unit.

The secondary velocity contours at the outlets of the 70° bifurcation with circular or semi-circular daughters are qualitatively similar indicating that flow path curvature itself establishes the qualitative features of the secondary flow field in a bifurcation. A comparison of the secondary velocity contours in the two above-mentioned flow units also shows that the change of cross-sectional shape causes an increase in the secondary flow strength while retaining the basic secondary flow pattern (Dean-type circulation).

In Table 4, we listed the loss in static (Δp) and total (Δp_0) pressures across the different flow units (including straight sections following the module) involved in the transformation of a straight pipe into a bifurcation by "co-joining of two bent pipes" (Fig. 3). Table 5 shows the loss in pressures across the different geometries involved in the transformation of the straight pipe into a bifurcation by the "splitter in a pipe" method (Fig. 4).

The placement of a splitter plate along a diameter of a straight pipe, so as to generate a 0° bifurcation with semi-circular daughter branches, results in a significant increase in both Δp and Δp_0. This may be attributed to the development of the additional boundary layers on both sides of the splitter plate. The introduction of flow path curvature into the above geometry, leading to the formation of a bifurcation with semi-circular daughter branches, results in a small increment in both Δp and Δp_0. This indicates that curvature in the presence of flow division effects does not affect the pressure losses appreciably. The change of cross-sectional shape in the daughter branches of the above geometry from semi-circular to circular, resulting in the formation of a bifurcation with circular daughter branches is found to cause a small decrement in the pressure losses. If, on the other hand, the straight pipe with

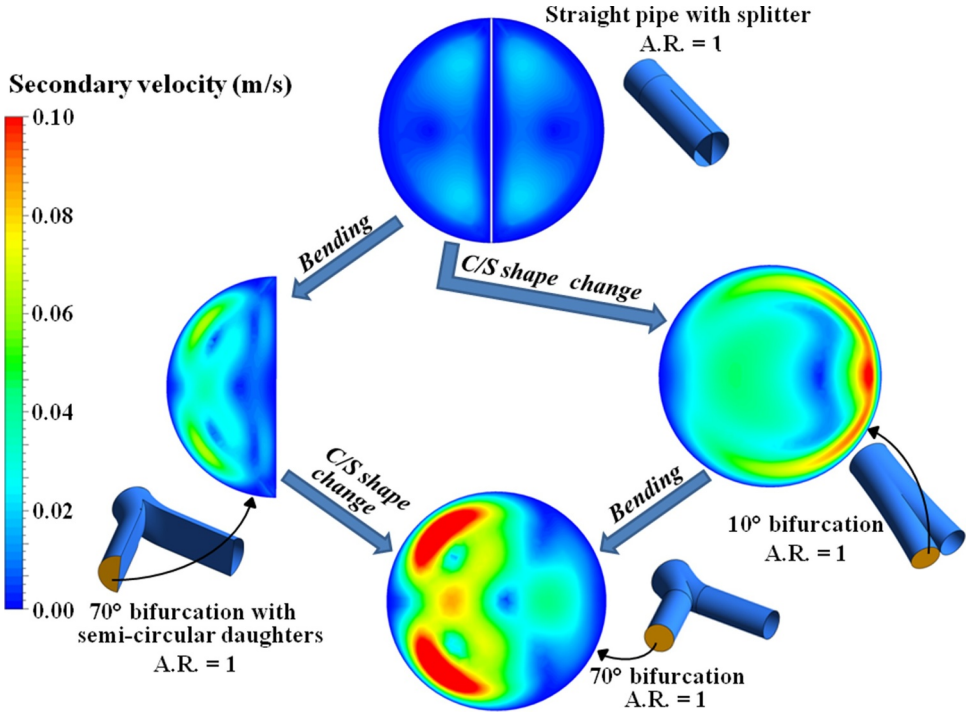

Fig. 14. Contours of secondary velocity magnitude at the outlet section of the various geometries involved in the construction of a bifurcation from a straight pipe (as shown in Fig. 4) for V_{inlet} = 1.46 m/s and A.R. =1.

splitter plate first undergoes a change of shape to form a bifurcation of (of small angle), both Δp and Δp_0 are found to decrease appreciably. The introduction of curvature at this stage results in a significant increase of both Δp and Δp_0. From the above discussion, it may be concluded that the curvature of flow path affects the pressure loss significantly provided the cross-section in the daughter branches is circular, while the change of cross-sectional shape in the daughter branches alters the pressure loss significantly in the absence of curvature effects.

5.3. Effects of the inlet velocity profile on the flow in a bifurcation

Here, we investigate the detailed anatomy of the three-dimensional modifications to the primary and secondary flow fields as the flow progresses through the intricate internal passage of a bifurcation. While many computations in this paper are performed with uniform inlet flow, several other inlet velocity profiles are considered in this section for comparative purposes. The case of paraboloidal inlet velocity is considered first in this context. As a visual aid to the overall characteristics of the flow, the primary velocity contours on the meridional plane (the plane passing through the centreline of the mother and two daughter branches) are constructed in Fig. 15. In order to represent the two cases with the same velocity scale and to be able to reveal appreciable flow details in both sets, the maximum velocity in the contour coloring scheme has been adjusted. It is evident from Fig. 15 that the velocity field in the daughter branches exhibit considerable asymmetry. The paraboloidal inlet velocity results in much greater asymmetry of velocity in the daughter branches as compared to a uniform inlet velocity. It is observed in Fig. 15 that for a fixed inlet flow rate, a change of the inlet velocity distribution from uniform to paraboloidal leads to a visible thickening of the boundary layer along the outer edges, and a thinning of the boundary layer formed along the inner edges. While the maximum velocity on the meridional plane occurs along the centreline of the mother branch for a paraboloidal inlet velocity, it is shifted towards the walls for a uniform inlet flow. It is observed that the region of low primary velocity created by the bifurcation ridge is much larger in the case of uniform inlet flow as compared to that for the paraboloidal inlet velocity.

Having studied the primary flow distribution on the meridional plane of the bifurcation flow unit for a uniform or paraboloidal inlet velocity distribution, we now investigate the evolution of the velocity field on successive cross-sectional planes in the same unit. Fig. 16 show how the variation of the cross-sectional shape (stations ‘a’ - ‘d’) in the three-dimensional internal passages of a bifurcation (A.R. = 1 and $\theta = 70°$) modify the flow field. This introduces additional complexities that are not encountered in curved pipes.

In order to capture the secondary motion at a cross-sectional plane properly, the planes have been constructed following the method that was described by Guha and Pradhan (2017). The cross-section at the inlet to the bifurcation module is circular. Station ‘a' (in Fig. 16) lies midway between the inlet and the plane passing through the concurrent point of the central axes of the three branches associated with module.

Table 5
Decrease of the area-averaged static pressure and mass-flow-averaged total pressure across different flow units involved in the construction of a bifurcation flow unit from a straight pipe (as shown in Fig. 4) for V_{inlet} = 1.46 m/s and A.R. = 1.

Geometry	Static pressure drop Δp (Pa)	Total pressure drop Δp_0 (Pa)
Straight pipe (inlet diameter equal to that of bifurcation)	1.0942	0.5779
Straight pipe with splitter	1.6746	0.9333
70° bifurcation with semi-circular daughters	1.7253	0.9966
10° bifurcation with circular daughters	1.2416	0.6659
70° bifurcation with circular daughters	1.7175	0.9897

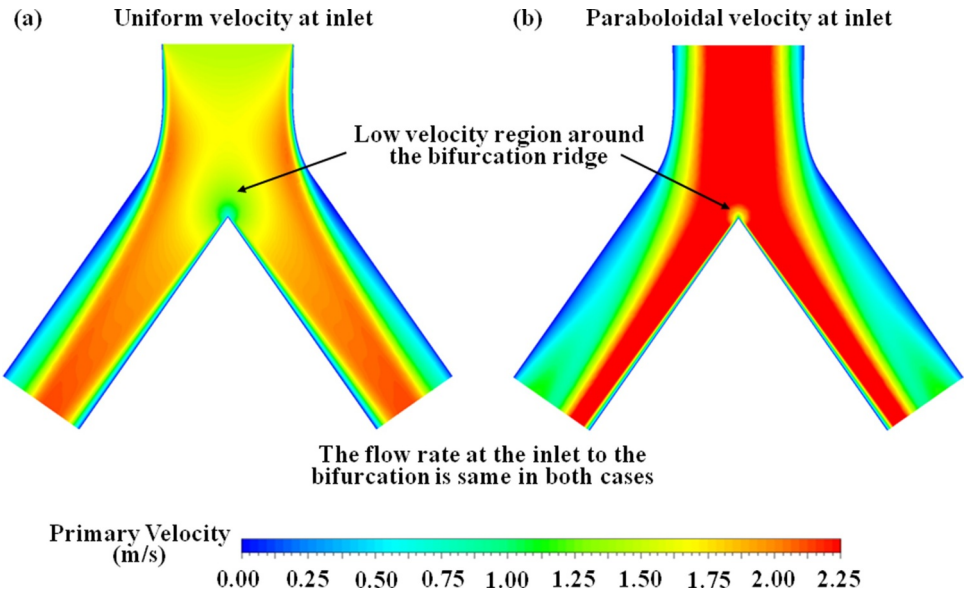

Fig. 15. Contours of primary velocity on the meridional plane of the bifurcation flow unit (A.R. =1) for two inlet velocity distributions. (a) uniform velocity V_{inlet} = 1.46 m/s, (b) paraboloidal velocity V_{avg} = 1.46 m/s.

Although the cross-sectional area at station 'a' is equal to that at the inlet, the shape is oval instead of circular (as was described in Fig. 1). At station 'b', two planes (subtending an angle of 170° on the upstream side) are present whose area normals subtend an angle of 10° with the area normal at station 'a'. Station 'd' corresponds to the end of the curved path of the bifurcation, and the area normal there makes an angle of 35° with the area normal at station 'a'. Station 'c' is defined midway between 'a' and 'd' such that its area normal makes an angle of 17.5° with respect to the centreline of the mother branch. The cross-section at station 'c' also consists of two planes (which subtend an angle of 145° on the upstream side). Station 'g' corresponds to the end-plane of the left daughter branch, and stations 'e' and 'f' are located at uniform intervals of centreline distance between stations 'd' and 'g'. The traces of the bifurcation ridge shown in Figs. 16–19 are the projection of the bifurcation ridge on the respective cross-sectional planes, the actual bifurcation ridge exists further downstream. In order to represent the two cases (of uniform and paraboloidal inlet velocities) with the same velocity scale and to be able to reveal appreciable flow details in both sets, the maximum velocity in the contour coloring scheme has been adjusted. Figs. 16 and 18 use the same velocity scale, the same is true for Figs. 17 and 19.

Fig. 16 shows the secondary velocity vectors superposed on the contours of primary velocity for a prescribed uniform inlet velocity. Owing to the uniform inlet velocity and the bifurcation ridge, the

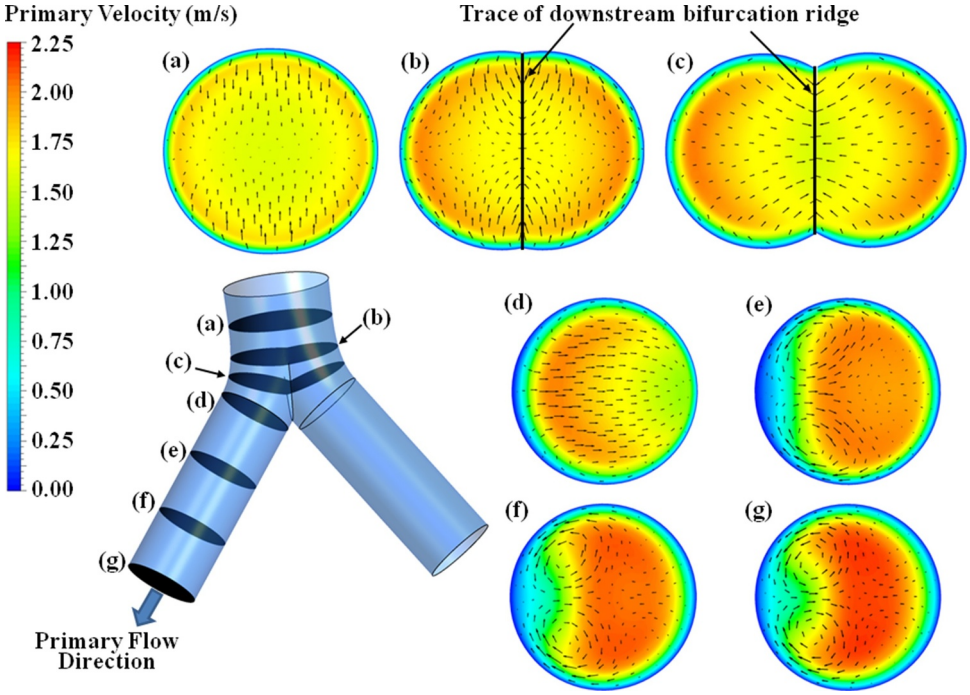

Fig. 16. Primary velocity contours with superposed secondary velocity vectors at intermediate cross-sections in a bifurcation flow unit (A.R. =1) for uniform inlet flow (V_{inlet} = 1.46 m/s). (The length of the vectors on any cross-sectional plane indicates the secondary velocity scaled by the respective maximum secondary velocity on that plane).

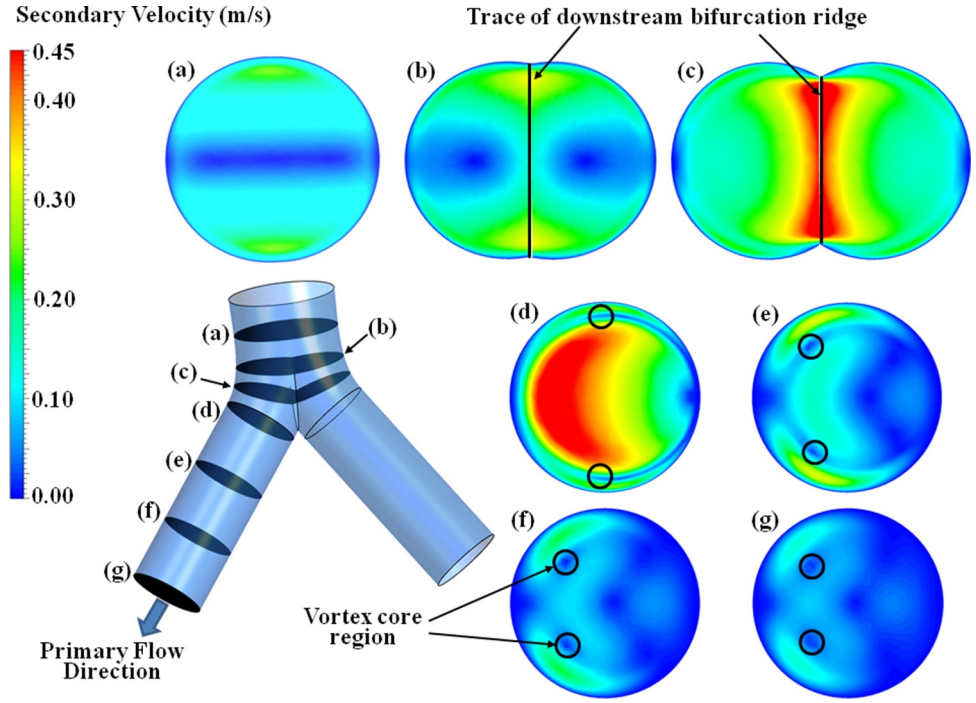

Fig. 17. Secondary velocity magnitude contours at intermediate cross-sections in a bifurcation flow unit (A.R. =1) for uniform inlet flow (V_{inlet} = 1.46 m/s).

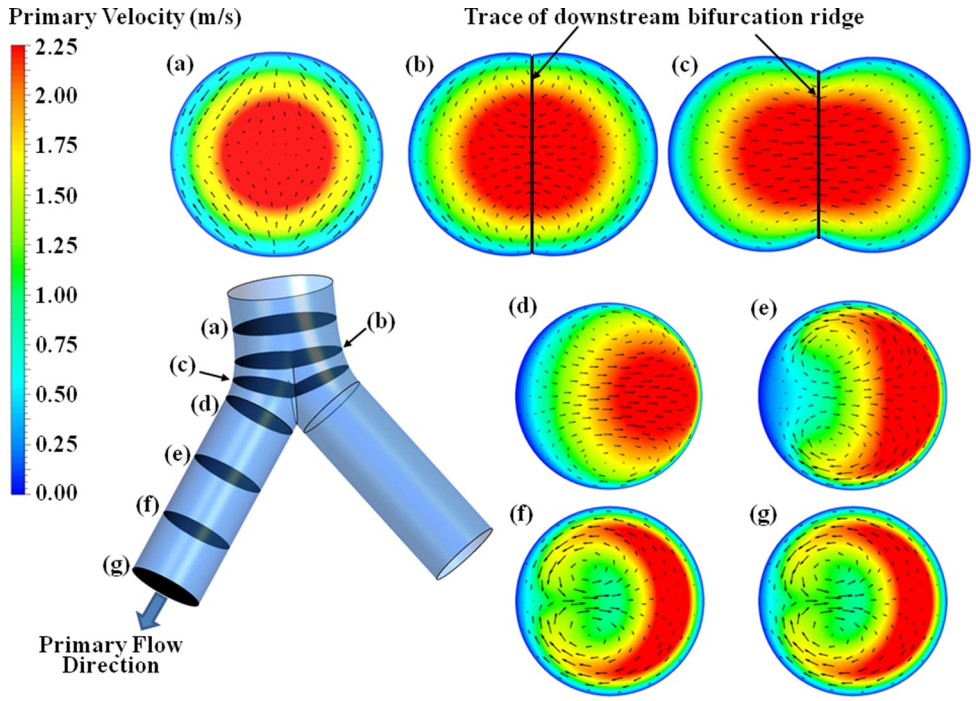

Fig. 18. Primary velocity contours with superposed secondary velocity vectors at intermediate cross-sections in a bifurcation flow unit (A.R. =1) for a paraboloidal velocity distribution at inlet with V_{avg} = 1.46 m/s.

maximum velocity at station ‘a' occurs in the peripheral regions of the cross-section instead of the usual central maximum observed in Poiseuille flow. The secondary flow at station ‘a' shows inward motion of fluid from the peripheral regions mainly caused by the change of shape from circular to oval. While the primary velocity contours at station ‘b' are qualitatively similar to those at station ‘a', the secondary flow pattern is different. The changing cross-sectional shape from station ‘a' to station ‘b' results in the motion of fluid from near the upper and lower edges towards the center of the cross-section at station ‘b'. At the central regions, two opposite tendencies are superposed: there is a tendency of setting up a secondary flow due to curvature effects from the outer edges towards the inner edges, whereas an opposite tendency exists because of the presence of the bifurcation ridge (with a region of low primary velocity in its vicinity). As a result of the above-mentioned up-down and sideways motion, a saddle-point type pattern is observed in the secondary motion at station ‘b' for uniform inlet flow (Fig. 16). The primary velocity contours at station ‘c' are qualitatively similar to those at the station ‘b' while the secondary flow pattern shows distinct fluid motion from the outer edges towards the inner edges, i.e. towards the center of the cross-section at station ‘c'. The curvature effects dominate

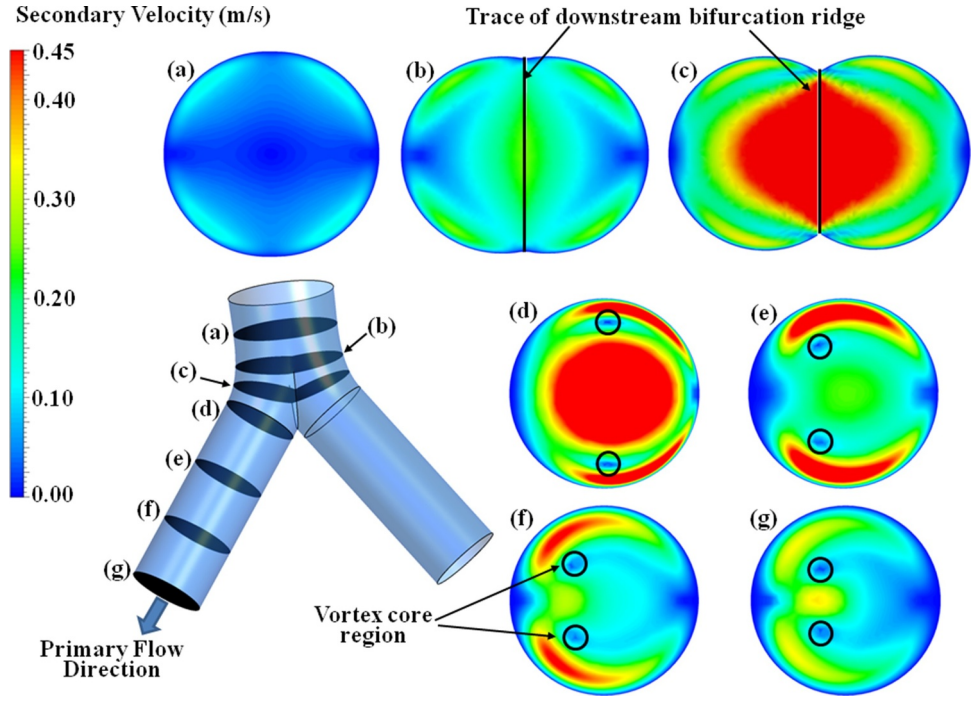

Fig. 19. Secondary velocity magnitude contours at intermediate cross-sections in a bifurcation flow unit (A.R. =1) for a paraboloidal velocity distribution at inlet with V_{avg} = 1.46 m/s.

over the effects of flow division here, resulting in the secondary motion driving fluid towards the inner edge.

The primary velocity contours at station ‘d' (which marks the start-plane of the left daughter branch) are characterized by a maxima near the outer edge of the bifurcation with typical Dean-type secondary flow. While the location of the maximum primary velocity (different to that observed in curved pipes) occurs due to the generation of a low velocity region around the bifurcation ridge and the velocity distribution just upstream of the ridge, the Dean type secondary motion occurs mainly due to curvature effects. The contours of primary velocity at stations ‘e', ‘f' and ‘g' show a gradual transformation of the velocity distribution resulting in the shift of the maximum from near the outer edge (at station ‘d') towards the inner edge (at station ‘g'). The contour at station ‘g' is similar to that reported in studies of flow in curved pipes, indicating that the straight section (between stations ‘d' and ‘g') following the bifurcation module tends to attenuate the effects introduced by flow division in a bifurcation. The secondary flow pattern at stations ‘e', ‘f' and ‘g' are qualitatively similar to that at station ‘d' with typical Dean type circulation, though with a significant shift in the position of the vortices towards the center (slightly towards the outer edge of the bifurcation) at station ‘g'.

Fig. 17 shows the secondary velocity contours for a prescribed uniform inlet velocity. $|\vec{v_S}|$ at station ‘a' is small, with the maximum occurring near the upper and lower walls due to the changing cross-sectional shape from circular to oval. The secondary velocity contours at station ‘b' are also characterized by maxima near the top and bottom walls and low $|\vec{v_S}|$ zones near the horizontal centreline. While the occurrence of the maxima is due to the change of cross-sectional shape, the regions of low $|\vec{v_S}|$ (stagnation regions of secondary flow) develop as a result of the mutual interaction of curvature effects with the effects of the bifurcation ridge (as explained in the context of Fig. 16). At station ‘c', $|\vec{v_S}|$ is much greater than that at the previous stations due to the significantly greater effect of flow path curvature at this station as compared to previous stations. Although flow division effects tend to generate secondary motion in a direction opposite to that induced by the curvature effects, the strength of the secondary flow induced by flow division effects is much smaller than that induced by curvature effects. Therefore, a significant increase in $|\vec{v_S}|$ takes place when curvature effects become dominant. The maximum secondary velocity occurs near the center at station ‘c' and this maximum shifts towards the outer edge (in both daughters) at station ‘d'. While the occurrence of the maxima near the cross-sectional center at station ‘c' may be attributed to curvature effects, the outward shift of the maxima at station ‘d' is due to the basic nature of Dean type circulation (existence of maximum secondary velocity near the cross-sectional center in the daughters in a bifurcation (Guha and Pradhan, 2017; Comer et al., 2001)) which develops there.

As the fluid traverses the straight cylindrical section following the bifurcation module (stations ‘e' - ‘g'), the $|\vec{v_S}|$ decreases considerably with a shift of its maximum value towards the upper and lower walls. It was shown by Guha and Pradhan (2017) that a region of small $|\vec{v_S}|$ in the interior of the cross-section (which usually appears in pairs) maps to vortex cores. In the present study, the λ_2-method (Jeong and Hussain, 1995) has been used for locating the vortex cores, and verify the above-mentioned statement. The methodology is described in Guha and Pradhan (2017), and the cores of the vortices thus identified are shown in Fig. 17. The dark blue regions (labeled in the figure with solid circles) occurring in pairs at stations ‘e' - ‘g' correspond to the cores of the Dean vortices found at the same locations in Fig. 16. Thus, the contours in Fig. 17 show that the cores of the Dean vortices tend to shift towards the horizontal centreline as the fluid traverses the straight section following the bifurcation module.

Fig. 18 shows the secondary velocity vectors superposed on the primary velocity contours for a prescribed paraboloidal inlet velocity. The same inlet flow rate has been kept as in the case of uniform inlet velocity to make direct comparisons possible. Owing to the prescribed paraboloidal velocity at the inlet the maximum velocity at station ‘a' occurs at the center. The secondary flow pattern at station ‘a' is similar to that observed for the uniform inlet flow. While the contours of primary velocity at station ‘b' are qualitatively similar to those at station ‘a', the secondary flow pattern shows fluid movement towards the inner edge of bifurcation. Unlike in the case of uniform inlet velocity (Fig. 16) where there was an interplay between the curvature and flow division effects, the curvature effects seem to mask the other effects in case of

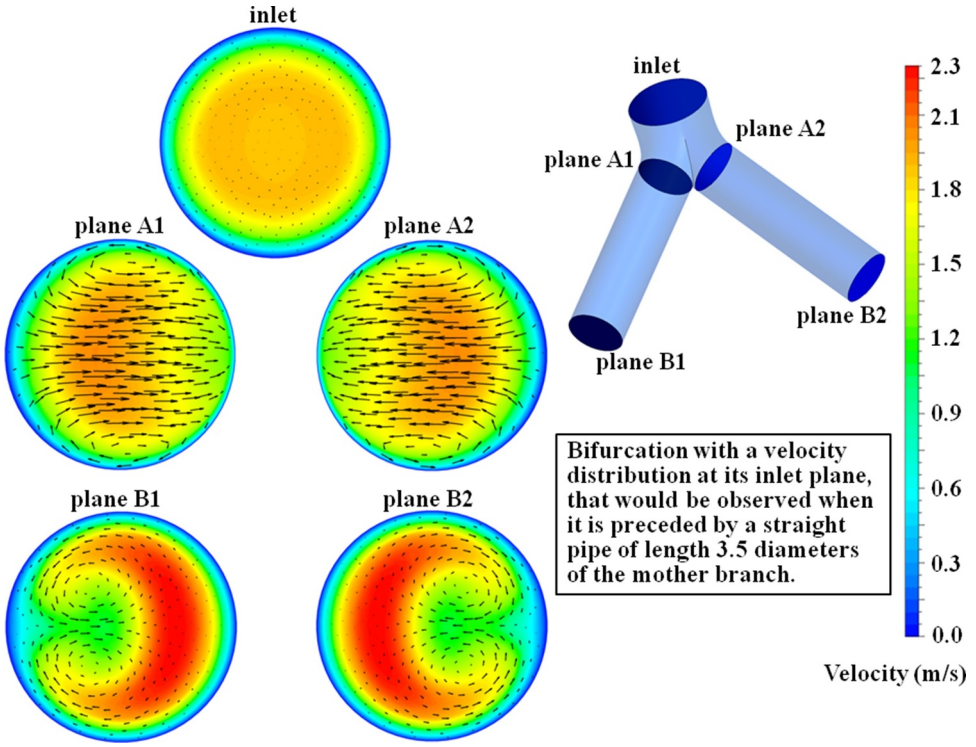

Fig. 20. Modification to the three-dimensional flow field caused by a bifurcation flow unit for an axisymmetric velocity distribution (V_{avg} = 1.46 m/s) at inlet that may be generated due to the presence of an upstream straight pipe: Vectors of secondary velocity superposed on the contours of primary velocity at selected cross-sectional planes in a bifurcation flow unit (A.R. =1). [The lengths of the secondary vectors indicate the magnitude of secondary velocity at a cross-section].

the paraboloidal inlet velocity (Fig. 18). Hence, no saddle-point type pattern is observed in the secondary motion at station 'b' for paraboloidal inlet flow. The changes in the primary velocity contours as well as the secondary flow pattern between stations 'b' and 'c' are found to be small.

Unlike the case of uniform inlet velocity, Fig. 18 shows that the contours of primary velocity at station 'd' are characterized by a high velocity region near the inner edge of the bifurcation. This may be attributed to the non-uniform (paraboloidal) inlet velocity distribution and the enhanced curvature effects under such a condition. The secondary flow pattern at station 'd' shows typical Dean type circulation. As the fluid traverses the straight section between stations 'd' and 'g', the primary velocity contours show the development of a crescent shaped region of high magnitude near the inner edge of the bifurcation and a shift of the Dean vortices towards the horizontal centreline. Comparing the features revealed in Figs. 16 and 18, it may be concluded that a change of the inlet velocity distribution from uniform to paraboloidal results in an increase of asymmetry in the velocity distribution at a cross-section, and a shift of the Dean vortices in the daughter branches (stations 'e' - 'g') from near the top and bottom walls on the outer edge side of the cross-section towards the horizontal centreline at the center of the cross-section.

Fig. 19 shows the secondary velocity contours for a paraboloidal inlet velocity. The strength of the secondary flow at stations 'a' and 'b' are smaller for the paraboloidal inlet velocity (Fig. 19) as compared to that for the uniform inlet velocity (Fig. 17). The stagnation regions that were observed in Fig. 17 at station 'b' appear shifted towards the walls in Fig. 19 and are less prominent due to the smaller values of $|\vec{v_s}|$ there. The average secondary velocity at station 'c' in Fig. 19 is considerably greater than that at the same location for the uniform inlet velocity case.

The secondary velocity at station 'd' for the paraboloidal inlet velocity is characterized by a region of high magnitude at the center of the cross-section (basic nature of Dean type circulation) and two other regions of considerable magnitude near the top and bottom walls. Fig. 19 also shows that the secondary flow strength at stations 'e' - 'g' are significantly greater for the paraboloidal inlet velocity as compared to the uniform inlet velocity (Fig. 17). Moreover, the paraboloidal inlet velocity results in the persistence of considerable secondary fluid motion even at station 'g'. The cores of the vortices shown in Fig. 19 (stations 'd' - 'g') are identified by using the λ_2-criterion, as stated previously in connection with Fig. 17. From the above discussion it may be concluded that non-uniformity in the inlet velocity distribution leads to the generation of greater secondary velocities in the bifurcation module, and the persistence of such motion up to further distances in the straight section following the bifurcation module.

Having discussed the evolution of the flow field in a bifurcation module when the velocity distribution at its inlet is uniform or paraboloidal (both being axisymmetric in nature), we explore an additional axisymmetric and two more skewed (i.e. non-axisymmetric) inlet velocity profiles that are relevant in the context of a branching network. The additional axisymmetric profile would arise at the inlet of the bifurcation module if the uniform velocity condition is applied at the inlet of a straight pipe of length 3.5 times the diameter of the mother branch that precedes the bifurcation module (resembling the straight section of a branch of the preceding generation in a network (Guha et al., 2016)). The two skewed profiles are named as profile I and profile II for a streamlined discussion. The skewed profile I consists of a non-uniform skewed velocity distribution with secondary motion that may arise at the inlet of the bifurcation module under consideration if a uniform velocity condition is applied at the overall inlet of an extended network in which two additional bifurcation modules exist upstream of the bifurcation module under consideration. The skewed profile II consists of a non-uniform skewed velocity distribution with secondary motion that would arise at the inlet of the bifurcation module under consideration if a paraboloidal velocity condition is applied at the overall inlet of an extended network in which an additional bifurcation module exists upstream of the bifurcation module under consideration. The adoption

of the two skewed profiles is an attempt, in a generic study like the present one, to capture the essence of the behavior of a bifurcation module when it is not isolated but operates within a branching network.

Fig. 20 shows the vectors of secondary velocity superposed on the contours of primary velocity at selected cross-sectional planes in a bifurcation flow unit of A.R. =1, for the case where an additional unit of length 3.5 times the diameter of the mother branch is introduced upstream of the bifurcation. In this case the velocity distribution at the inlet plane of the bifurcation unit is neither uniform nor paraboloidal, but approximately corresponds to the velocity distribution that would exist within the developing length in a pipe at 3.5D from the inlet (where a uniform velocity is specified). Since the bifurcation is geometrically symmetric and the velocity field at the inlet plane of the bifurcation module is symmetric about the bifurcation ridge, the flow field in the two daughter branches are mirror images of one another (this feature was also present in the case of uniform and paraboloidal inlet velocity profiles described above). Fig. 20 may be considered in conjunction with Figs. 16 and 18 to comprehend the effects of various axisymmetric inlet velocity profiles on the flow structure in a bifurcation module.

The primary velocity contours at plane A1 (which marks the start-plane of the left daughter branch and corresponds to station 'd' in Figs. 16 and 18) are characterized by a crescent shaped high velocity region near the center of the cross-section with typical Dean-type secondary flow. While the maximum velocity was located near the outer edge of the bifurcation for the uniform inlet velocity, and near the inner edge of the bifurcation for the paraboloidal inlet velocity, in this case, the maximum velocity is found to occur near the center of the cross-section. The primary velocity contours at plane B1 (which is a cross-sectional plane 3.5 diameters downstream of plane A1 and corresponds to station 'g' in Figs. 16 and 18) show the characteristic skewed nature, with the degree of cross-sectional non-uniformity lying between that observed for the uniform inlet velocity and paraboloidal inlet velocity cases. The secondary flow pattern at plane B1 is qualitatively similar to that at the same plane for the uniform and paraboloidal inlet velocity cases.

Fig. 21 shows the vectors of secondary velocity superposed on the contours of primary velocity at selected cross-sectional planes in a bifurcation flow unit of A.R. =1, when the skewed profile I is specified at the inlet to the bifurcation. The inlet velocity distribution, given in Fig. 21, thus shows a skewed nature with Dean-type secondary circulation. Owing to the asymmetry in the velocity distribution at the inlet with respect to the bifurcation ridge, the flow fields in the two daughters develop differently (even though the two daughters are geometrically identical). The maximum (and average) velocity in the left daughter branch is significantly greater than that in the right daughter branch due to the particular skewed nature of the inlet flow. Although the velocity contours at plane A1 appear to be qualitatively similar to that observed in the previous case (Fig. 20), the contours at plane B1 appear different. The velocity contours and the secondary flow pattern in the right daughter branch (planes A2 and B2) appear quite different from those in the left daughter branch (planes A1 and B1). While the two dominating vortices in planes A1 and B1 are of the Dean type, two anti-Dean type vortices mark the dominating feature in planes A2 and B2. The two anti-Dean vortices form near the horizontal centreline of the cross-section at plane A2, whose strength significantly diminishes at plane B2.

Fig. 22 shows the changes in the flow field across a bifurcation flow unit when the skewed profile II is specified at its inlet. Owing to the asymmetry in the velocity distribution at the inlet with respect to the bifurcation ridge, the flow fields in the two daughters develop differently with the maximum (and average) velocity in the left daughter branch being significantly greater than that in the right daughter branch. The primary velocity at plane A1 shows a skewed nature with the maximum velocity shifted towards the outer edge of the bifurcation (as was found for the uniform inlet velocity case in Fig. 20). Fig. 22 shows that the velocity contours at plane B1 are different from those found at the same locations for the other inlet velocity profiles considered in this study; the primary velocity has two distinct maxima near the top and bottom edges. The primary velocity contours at planes A2 and B2 in Fig. 22, on the other hand, appear similar to that at the same location in Fig. 21 (i.e. for the skewed profile I).

The secondary flow patterns shown in Fig. 22 show the existence of two pairs of counter-rotating vortices (two Dean and two anti-Dean type) at planes A1 and A2. The secondary flow field at plane B1 shows a single pair of vortex (anti-Dean type) whereas the strength of the vortices in the right daughter branch diminishes to such an extent that no vortical structures are discernible at plane B2. This is in contrast to the observation made for the skewed profile I in Fig. 21 where plane B1 showed the presence of a Dean vortex pair and an anti-Dean pair was clearly visible at plane B2.

A comparison of Figs. 16, 18, 20, 21 and 22 shows that the inlet velocity distribution has a significant impact on the flow field in the bifurcation module. As an example, asymmetry in the inlet profile of primary velocity with respect to the bifurcation ridge (as are the cases shown in Figs. 21 and 22) results in unequal flow distribution among the daughter branches (although they are geometrically identical). Similarly it is found that, when a helical motion (i.e. secondary motion along with the primary flow) is prescribed at the inlet (as are the cases shown in Figs. 21 and 22), the anti-Dean type secondary motion may be produced just in a single bifurcation (Fig. 21) which is usually reported only in a large branching network (Guha and Pradhan, 2017) and did not appear in all other studies of a single bifurcation module where various profiles of primary velocity are prescribed at the inlet without any secondary motion there.

5.4. Determination of the fluid dynamic changes as the flow recovers in the daughter branches

In order to keep a study like the present one, where there are a large number of variables, tractable we have so far kept the length of the straight portion following the daughter branches such that the value of $L_{straight}/D_{daughter}$ is 3.5 (a commonly observed value in many natural/biological systems (Pedley et al., 1970a,b, 1971)). In this section, we allow much greater length of the straight portion and study how the flow field evolves to the Poiseuille-type configuration. The evolution of the contours of primary velocity are plotted at various locations downstream of the bifurcation (denoted by nD indicating the distance from the end-plane of the bifurcation in terms of the daughter branch diameter) with the vectors of secondary velocity superposed on the contours. In the next two diagrams, the lengths of the secondary velocity vectors are proportional to the strength of secondary motion. Owing to the symmetry of the flow field (the flow field in the two daughters are mirror images of one another), the flow structure in only the left daughter branch is discussed here.

Fig. 23 shows the flow field in the left daughter branch for a uniform velocity (V_{avg} = 1.46 m/s) at the inlet of the bifurcation module. It is found that the Poiseuille-type paraboloidal velocity distribution is recovered at about 30 diameters downstream of the bifurcation. It is found that the primary velocity at the end-plane of the bifurcation module (i.e. at $n = 0$ in Fig. 23) is characterized by a high velocity region near the outer edge of the bifurcation due to the development of a low velocity region around the bifurcation ridge. The location of this high velocity region shifts towards the inner edge of the bifurcation as the flow proceeds downstream (owing to curvature effects), and finally returns to a central location as the secondary flow decreases in strength. Thus, the region of high velocity shifts from the outer toward the inner edge (crossing the center of the cross-section in this journey) and then moves back to the center. It is also interesting to note how the shape of this high velocity region changes as the flow proceeds downstream, from being almost semi-circular at $n = 1$ to a distinct crescent shape at about $n = 6$, to circular at $n \geq 20$. Fig. 23 shows that the secondary

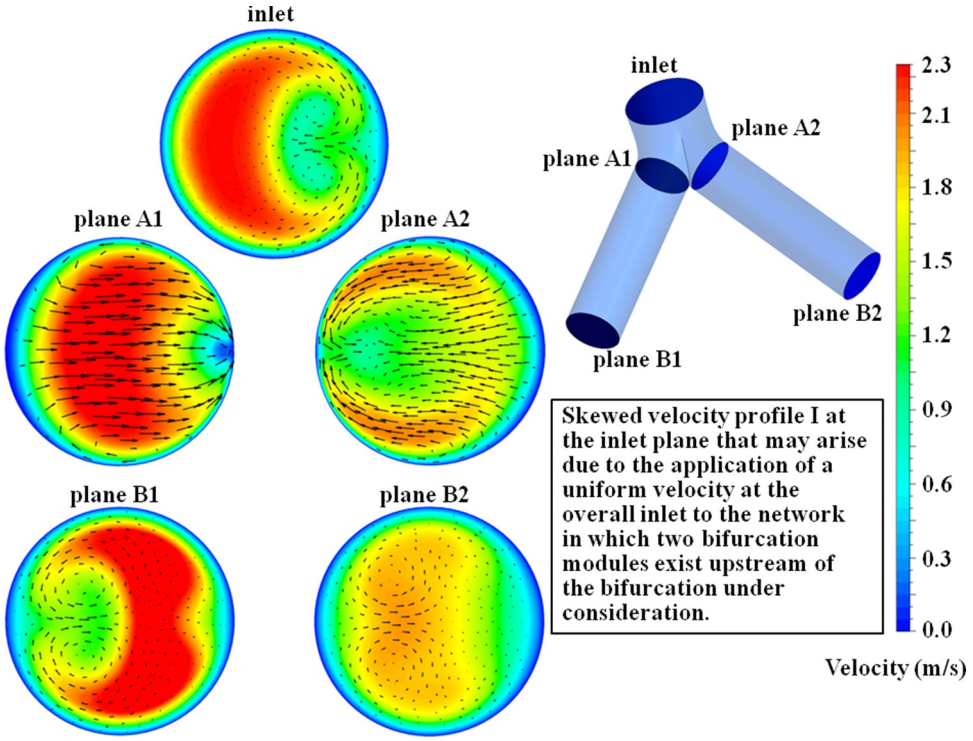

Fig. 21. Modification to the three-dimensional flow field caused by a bifurcation flow unit for the skewed velocity profile I (V_{avg} = 1.46 m/s) at the inlet: Vectors of secondary velocity superposed on the contours of primary velocity at selected cross-sectional planes in a bifurcation flow unit (A.R. =1). [The lengths of the secondary vectors indicate the magnitude of secondary velocity at a cross-section].

flow is characterized by typical Dean-type circulation (Guha and Pradhan, 2017). The two counter-rotating Dean vortices are visible up to $n = 6$, beyond which no distinct pattern of the secondary flow can be discerned. The strength of secondary circulation decreases rapidly, and becomes quite insignificant at about 10 diameters downstream of the bifurcation ($n = 10$), although the vortex patterns may still be visualized afterwards by appreciably magnifying the lengths of the vectors.

Fig. 24 shows the flow field in the left daughter branch for a

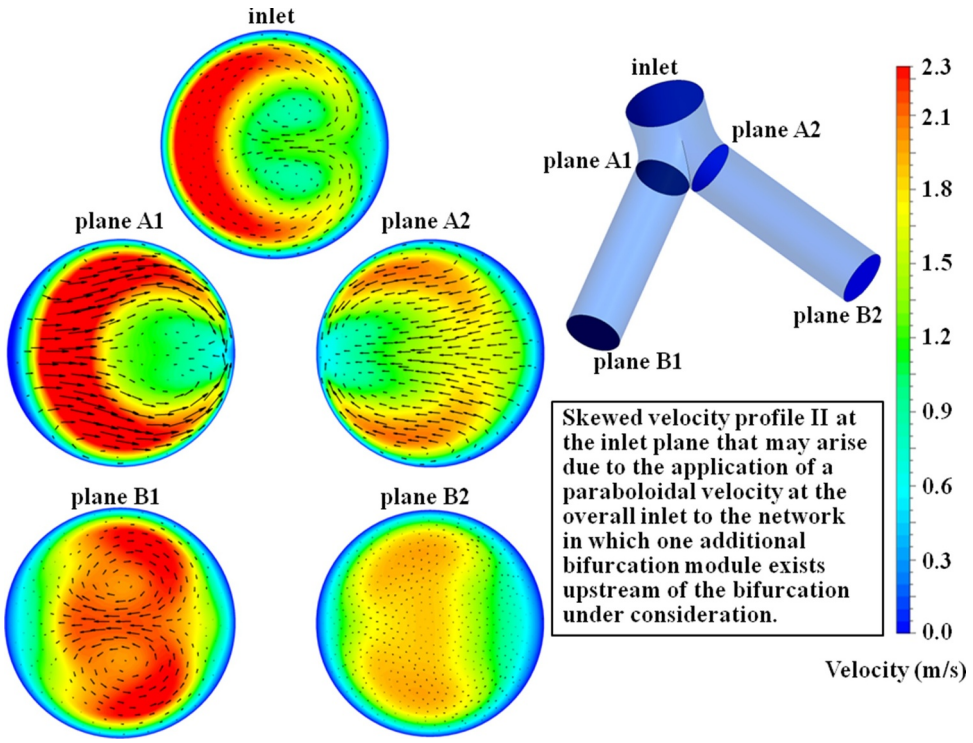

Fig. 22. Modification to the three-dimensional flow field caused by a bifurcation flow unit for the skewed velocity profile II (V_{avg} = 1.46 m/s) at the inlet: Vectors of secondary velocity superposed on the contours of primary velocity at selected cross-sectional planes in a bifurcation flow unit (A.R. =1). [The lengths of the secondary vectors indicate the magnitude of secondary velocity at a cross-section].

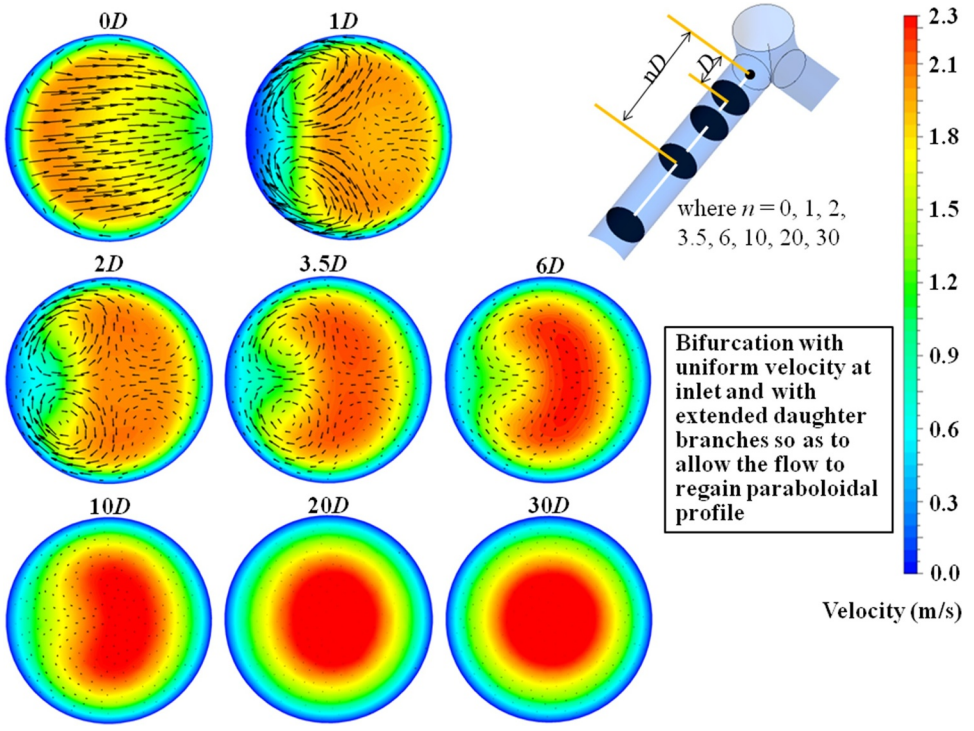

Fig. 23. Physics of the process of equilibration of the flow field created by a bifurcation module: Vectors of secondary velocity superposed on the contours of primary velocity at selected cross-sectional planes in the straight section following a bifurcation module (A.R. =1) for a uniform velocity distribution (V_{inlet} = 1.46 m/s) at inlet. [The lengths of the secondary vectors indicate the magnitude of secondary velocity at a cross-section].

paraboloidal velocity (V_{avg} = 1.46 m/s) at the inlet of the bifurcation module. It is found that the Poiseuille-type velocity distribution is recovered at about 50 diameters downstream of the bifurcation. In contrast to the case of uniform inlet velocity (Fig. 23), it is found that, for the paraboloidal inlet velocity, the primary velocity contours at the end-plane of the bifurcation module (i.e. at n = 0 in Fig. 24) display a high velocity region near the inner edge of the bifurcation. The shape of this high velocity region in the cross-section changes from being

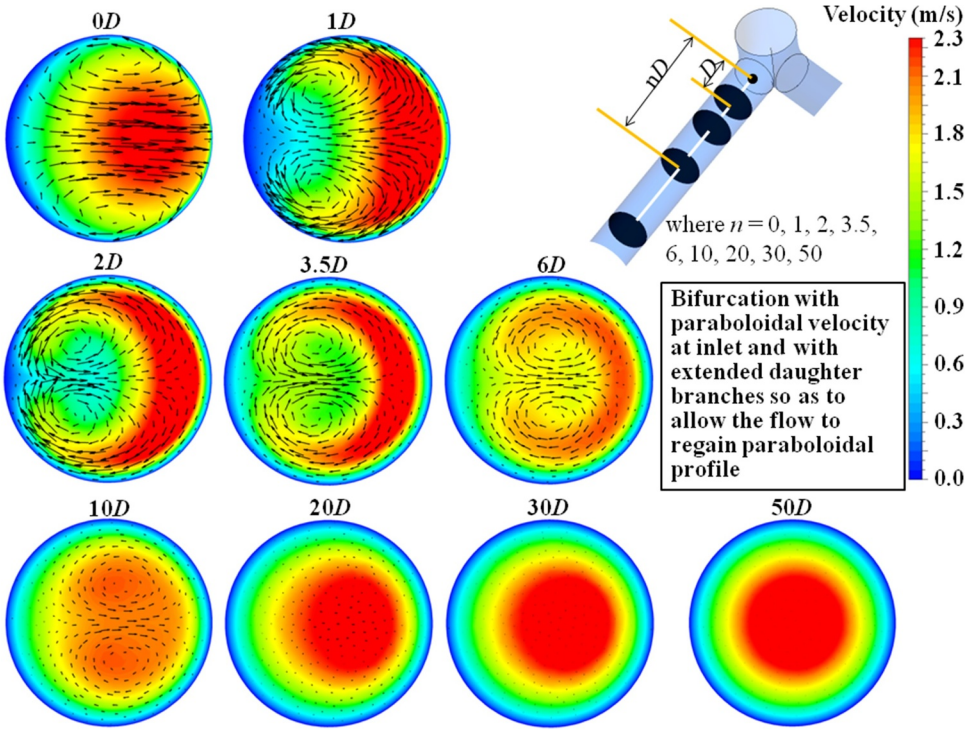

Fig. 24. Physics of the process of equilibration of the flow field created by a bifurcation module: Vectors of secondary velocity superposed on the contours of primary velocity at selected cross-sectional planes in the straight section following a bifurcation module (A.R. =1) for a paraboloidal velocity distribution (V_{avg} = 1.46 m/s) at inlet. [The lengths of the secondary vectors indicate the magnitude of secondary velocity at a cross-section].

crescent shaped at $n = 1$ to nearly circular (but not at the center of the cross-section) at $n = 20$. Then, the location of this circular high velocity region shifts towards the center of the cross-section as the flow proceeds downstream. While this journey of the location of the high velocity region is more straightforward here (as compared to the case of uniform velocity profile), the evolution of maximum velocity is more complex as it initially decreases up to about $n = 10$ and then increases again until the Poiseuille-type velocity distribution is regained. It is observed that the velocity field is skewed towards the inner edge of the bifurcation to a much greater extent in this case as compared to that for the uniform inlet velocity case. Calculations also show that the secondary flow strength at a given cross-section is greater for this case as compared to that for the uniform inlet velocity case. The vortical structures are seen to last for greater length in Fig. 24 as compared to that in Fig. 23. From the above discussion it may be concluded that the paraboloidal inlet velocity fosters greater degree of cross-sectional non-uniformity in the velocity distribution as well as aids in the persistence of secondary motion up to greater lengths downstream of the bifurcation. Consequently the length required to attain Poiseuille-type velocity distribution in the downstream branch is greater when the velocity at the inlet of the bifurcation module is paraboloidal. It may appear surprising at first sight that the three-dimensional flow modifications made by a bifurcation module are such that a transformation of paraboloidal at inlet to paraboloidal velocity distribution in a daughter branch takes longer distance than a transformation of uniform to paraboloidal velocity distribution.

5.5. Pressure losses associated with a bifurcation

Experimental determination of the pressure drop across a bifurcation is difficult because the variation of pressure across a cross-section is comparable to the overall downstream decrease in pressure. Following the work of Pedley et al. (1970a,b, 1971), a “flow unit' is defined as a bifurcation module followed by straight sections along the two daughter branches (Fig. 2). In the present work, equivalent flow units are constructed for the constituent elements (e.g. bent or straight pipes) also. Pedley et al. (1970a,b, 1971) calculated the viscous dissipation occurring between two locations from velocity measurements along two perpendicular lines at each location. Their dissipation model had an implicit assumption that disturbances in the flow (which generate secondary motion) are created in a non-viscous manner in the bifurcation module and are dissipated in the following daughter tubes by the action of viscosity (Pedley et al., 1970a). We invoke the power of CFD to accurately determine the decrease of total pressure across a bifurcation module (Fig. 1) as well as that across a bifurcation flow unit (Fig. 2).

The loss of total pressure Eq. (4) across a flow module is denoted by $\Delta p_{0,\ geometry}$ while the loss of total pressure across straight sections following the module is denoted by $\Delta p_{0L,\ geometry}$, where the subscript '*geometry*' may be bifurcation, bent or straight depending on whether the straight section follows a bifurcation module, a bent pipe or a straight pipe respectively. Then, the overall loss of total pressure across the flow unit $\Delta p_{0t,\ geometry}$ (comprising the module followed by straight section/s) is given by

$$\Delta p_{0t,geometry} = \Delta p_{0,geometry} + \Delta p_{0L,geometry} \tag{8}$$

Three different geometries of bifurcation module (Table 1) were considered in Section 5.1. In order to make the study on pressure loss more comprehensive, several more geometries are added to this list, covering practically reasonable ranges of values for three geometric parameters, viz.$(L_1 + L_2)/D_{inlet}$, A.R. and θ. The complete list is given in Table 6 for ready reference. The three geometries of Table 1 are named by letters A, B and C in Table 6, whereas the new geometries are named by numerals 1–11. It was found that in order to ensure that the shape of the bifurcation is realistic, the value of $(L_1 + L_2)/D_{inlet}$ must be close to or greater than unity, while the values of A.R. are chosen based on the usual practices of various modeling techniques (Murray, 1926; Kitaoka et al., 1999). Bifurcation 1 represents a geometry that obeys Murray's law (Murray, 1926) of minimum losses while Bifurcation 3 represents a case when the A.R. is the inverse of that stipulated by Murray's law. Bifurcation 2 is based on the dimensions of generations G1-G2 of Weibel's model (Weibel, 1963) of the human bronchial tree. In Bifurcation 5, the diameter of the daughter branches is the same as that in Bifurcation 1 while the area ratio is equal to unity. Bifurcations 4 and 6 are constructed so as to cover a range of values of the geometric parameters $(L_1 + L_2)/D_{inlet}$ and A.R. In order to study the effect of the bifurcation angle (θ) on the fluid dynamics, θ is varied from 60° to 100° in Bifurcations 7 - 11. It was found that the variation of the bifurcation angle in the range $60° \le \theta \le 100°$ results in small changes of the velocity field as well as the pressure drops across the bifurcation.

Table 6
Geometric details of the different bifurcation modules considered in the present study.

Geometry	D_{inlet}(mm)	$(L_1 + L_2)/D_{inlet}$	Area Ratio (A.R.)	θ(°)
Bifurcation A	10.00	1.45	2.00	70
Bifurcation B	10.00	1.35	1.00	70
Bifurcation C	10.00	1.25	0.67 (= 2/3)	70
Bifurcation 1	10.00	1.30	1.26 ($=\sqrt[3]{2}$)	70
Bifurcation 2	12.20	1.33	0.93	70
Bifurcation 3	10.00	1.30	0.79 ($=1/\sqrt[3]{2}$)	70
Bifurcation 4	12.60	1.11	1.14	70
Bifurcation 5	11.23	1.16	1.00	70
Bifurcation 6	12.60	1.03	0.79($=1/\sqrt[3]{2}$)	70
Bifurcation 7	10.00	1.30	1.00	60
Bifurcation 8	10.00	1.30	1.00	70
Bifurcation 9	10.00	1.30	1.00	80
Bifurcation 10	10.00	1.30	1.00	90
Bifurcation 11	10.00	1.30	1.00	100

A “flow unit” (Fig. 2) consists of a bifurcation module followed by two daughter branches. Except otherwise stated, the value of ($L_{straight}/D_{daughter}$) which represents the total straight length of the daughter branches is kept at 3.5 (a commonly observed value in many natural/biological systems (Pedley et al., 1970a,b, 1971)).

Since we have considered the flow in generic bifurcations (Table 6) and the inlet Reynolds number is varied in the range 400 - 2000, the characteristics of pressure loss obtained here would be applicable to laminar flow in biological networks as well as in future engineered branching networks (based on fractal or other such algorithms). As an example, considering that turbulent effects are negligible in all generations downstream of G0 in human bronchial network at resting conditions and downstream of G5 for most breathing conditions, the present fluid dynamic results and conclusion would be relevant there.

Table 7 shows the loss in total pressure ($\Delta p_{0,\ bifurcation}$) across Bifurcation 5 and that across its equivalent straight ($\Delta p_{0,\ straight}$) and bent ($\Delta p_{0,\ bent}$) pipes for different inlet velocities in the range $0.58\ \text{m/s} < V_{inlet} < 2.32\ \text{m/s}$. It is found that $\Delta p_{0,\ bent} > \Delta p_{0,\ straight}$

Table 7
Variation of the loss of total pressure (Δp_0) with uniform inlet velocity across a bifurcation module (Bifurcation 5:$D_{inlet} = 11.23$ mm, A.R. = 1), an equivalent straight pipe and an equivalent bent pipe.

V_{inlet}(m/s)	$\Delta p_{0,\ straight}$(Pa)	$\Delta p_{0,\ bent}$(Pa)	$\Delta p_{0,\ bifurcation}$(Pa)
0.58	0.1384	0.1385	0.1045
0.87	0.2285	0.2295	0.1745
1.16	0.3286	0.3301	0.2522
1.46	0.4356	0.4392	0.3360
1.74	0.5494	0.5549	0.4249
2.03	0.6695	0.6769	0.5184
2.32	0.7958	0.8049	0.6161

for the range of flow rates considered, the difference between the two increasing as V_{inlet} increases. The curvature of flow path is thus responsible for an increase of the loss of total pressure across the pipe. For the entrance flow in a straight pipe, the incurred loss is greater than that in the case of Poiseuille flow, and in the course of this work, we found that the loss incurred in the entrance region of a straight pipe may even be greater than that in the entrance region of a bent pipe when A.R. < 1. Such a feature may be attributed to the thinning of the boundary layer (where most of the loss occurs) on the inner edge in the entrance region of the bent pipe (Singh, 1974). Even more interesting is the fact that the loss in total pressure across the bifurcation module formed by joining two bent pipes (Fig. 3) is significantly smaller than that in the bent pipe alone. A contributory factor to this finding may be visualized by the partial removal of the internal wall in the formation of the bifurcation from the co-joining of two bent pipes.

The above discussion gives the impression that the losses associated with a symmetric bifurcation are lower than that in its equivalent straight and bent pipes. However, as mentioned previously, such a bifurcation in a branching network is usually followed by a pair of straight sections representing the daughter branches (Fig. 2). Further insight into the fluid dynamics of loss may thus be obtained by considering the loss of total pressure across the flow units (formed by adding straight sections after the bent pipe as well as the daughter branches of a bifurcation).

Table 8 shows the loss in total pressure across a flow unit ($\Delta p_{0t,\ bifurcation}$) constructed by adding straight sections at the end-planes of Bifurcation 5, and that across its constituent straight ($\Delta p_{0t,\ straight}$) and bent pipe ($\Delta p_{0t,\ bent}$) flow units for various inlet velocities. Use of Eq. (8), and the data given in Tables 7 and 8 show consistently that $\Delta p_{0L,\ bifurcation} > \Delta p_{0L,\ bent}$, while it was shown in Table 7 that $\Delta p_{0,\ bifurcation} < \Delta p_{0,\ bent}$ in the range of inlet flow rates considered here. In fact, $\Delta p_{0L,\ bifurcation}$ is sufficiently greater than $\Delta p_{0L,\ bent}$ such that $\Delta p_{0t,\ bifurcation}$ turns out to be greater than $\Delta p_{0t,\ bent}$ for most of the flow rates (except for $V_{inlet} = 0.58$m/s) considered here. This means that although the loss in total pressure across the bifurcation module is smaller than that across its constituent/equivalent pipes, the bifurcation has a greater potential for incurring losses in the following straight section as compared to that in the equivalent straight or bent pipes. Such a feature of the losses incurred by the flow in a bifurcation is attributable to the combined effects of asymmetry in the velocity field (which occurs as a result of flow path curvature and change of cross-sectional shape and area) and the generation of additional boundary layers along the inner edges of the bifurcation (which occurs due to flow division). Although $\Delta p_{0L,\ bifurcation} > \Delta p_{0L,\ bent}$ for all flow rates considered here, if the loss in just the bifurcation itself ($\Delta p_{0,\ bifurcation}$) is significantly smaller than that in the bent pipe itself ($\Delta p_{0,\ bent}$), then the overall loss of total pressure across the bifurcation flow unit ($\Delta p_{0t,\ bifurcation}$) may be smaller than the overall loss across the bent pipe flow unit ($\Delta p_{0t,\ bent}$). The smaller value of $\Delta p_{0t,\ bifurcation}$ as compared to $\Delta p_{0t,\ bent}$ at $V_{inlet} = 0.58$m/s (Table 8) may thus be attributed to the significantly smaller value of $\Delta p_{0,\ bifurcation}$ as compared to $\Delta p_{0,\ bent}$ (Table 7).

Table 8
Variation of the loss of total pressure (Δp_0) with uniform inlet velocity across a bifurcation flow unit (Bifurcation 5:$D_{inlet} = 11.23$ mm, A.R. = 1), an equivalent straight pipe unit and an equivalent bent pipe unit.

V_{inlet}(m/s)	$\Delta p_{0t,\ straight}$(Pa)	$\Delta p_{0t,\ bent}$(Pa)	$\Delta p_{0t,\ bifurcation}$(Pa)
0.58	0.2662	0.2802	0.2766
0.87	0.4335	0.4630	0.4687
1.16	0.6176	0.6665	0.6899
1.46	0.8143	0.8882	0.9383
1.74	1.0220	1.1266	1.2127
2.03	1.2401	1.3804	1.5125
2.32	1.4679	1.6492	1.8340

In Section 5.3, we studied the effect of inlet velocity distribution on the flow field generated in a bifurcation module. Five inlet velocity profiles were considered for the above purpose, of which three were axisymmetric profiles and the remaining two were skewed profiles. The axisymmetric profiles included the commonly used uniform and paraboloidal profiles, and a profile that would arise at the inlet of the bifurcation module if the uniform velocity condition is applied at the inlet of a straight pipe of length 3.5 times the diameter of the mother branch that precedes the bifurcation module. The two skewed profiles (I and II) consist of non-uniform primary velocity distribution with secondary motion at the inlet plane of the bifurcation, a situation that may arise in a branching network. Here, we determine the effect of the same inlet velocity profiles on the pressure loss in the bifurcation module and across straight sections following the module.

Table 9 shows the effects of the three axisymmetric inlet velocity profiles on the loss of total pressure across a bifurcation module and that across straight sections ($L_{straight}/D_{daughter} = 3.5$) following it. It is found that while $\Delta p_{0,\ bifurcation}$ for the paraboloidal inlet velocity is smaller than that for the uniform inlet velocity, $\Delta p_{0L,\ bifurcation}$ is significantly greater for the paraboloidal inlet velocity. This indicates that although the loss incurred within the bifurcation module is smaller for the paraboloidal case, a much greater potential for loss generation is developed there. This may be attributed to the greater degree of non-uniformity in the cross-sectional velocity distribution generated by the paraboloidal inlet velocity (compare Fig. 18d with Fig. 16d). Therefore, the loss of total pressure across the flow unit (comprising the bifurcation module as well as the straight sections of $L_{straight}/D_{daughter} = 3.5$) turns out to be greater for the case of paraboloidal inlet velocity. Table 9 also shows the values of pressure losses for the inlet velocity profile that is generated due to the presence of an additional upstream pipe of $L/D = 3.5$. It is found that the values of $\Delta p_{0,\ bifurcation}$ for this case are closer to those for the paraboloidal inlet velocity whereas the values of $\Delta p_{0L,\ bifurcation}$ for the same case are closer to those for the uniform inlet velocity.

Table 10 shows the values of $\Delta p_{0,\ bifurcation}$ and $\Delta p_{0L,\ bifurcation}$ for the two skewed inlet velocity profiles for a range of magnitudes of the average velocity. For $V_{avg} = 1.46$ m/s, the skewed velocity profile I at inlet plane is displayed in Fig. 21 and the skewed velocity profile II at inlet plane is displayed in Fig. 22. The values of $\Delta p_{0,\ bifurcation}$ for these cases are found to be closer to the uniform inlet velocity case. While $\Delta p_{0,\ bifurcation}$ for skewed profile I are smaller that those for the uniform velocity, the same for skewed profile II exceeds those for the uniform case for $V_{avg} \geq 0.87$m/s. Since the skewed velocity profile at the inlet results in unequal flow distribution among the two daughter branches, two values of $\Delta p_{0L,\ bifurcation}$ are quoted (one for each daughter) for this case. For skewed profile I, the value of $\Delta p_{0L,\ bifurcation}$ for the left daughter branch (which receives the major share of the flow from the mother branch) are found to lie approximately midway between the corresponding values for the uniform and paraboloidal cases; for skewed profile II, it is close to that for the paraboloidal case. For both skewed inlet velocity profiles, the value of $\Delta p_{0L,\ bifurcation}$ for the right daughter branch seem to be close to that for the third type axisymmetric inlet profile (with additional unit of 3.5D upstream) shown in Table 9.

Based on extensive computations for 9 different bifurcations (Bifurcations A-C and Bifurcations 1–6 in Table 6) at various flow rates (Tables 7–10) considering two types of inlet velocity profiles (uniform and paraboloidal), new correlations are proposed in the Appendix for estimating the loss across a bifurcation and the loss across a straight section following a bifurcation as functions of $(L_1 + L_2)/D_{inlet}$, A.R. and Re.

Now, we attempt to quantify the potential of the flow for incurring losses in the straight sections following the module. We define a loss potential ϕ for a given geometry as follows:

$$\phi = \Delta p_{0L,geometry} - \Delta p_{0L,\ straight} \quad (9)$$

Table 9
Variation of the loss of total pressure (Δp_0) with flow rate across a bifurcation module (Bifurcation 5:D_{inlet} = 11.23 mm, A.R. = 1) and across a straight section ($L_{straight}/D_{daughter}$ = 3.5) following the bifurcation module for three axisymmetric inlet velocity distributions.

V_{avg} (m/s) at inlet	$\Delta p_{0,\ bifurcation}$ (Pa)			$\Delta p_{0L,\ bifurcation}$ (Pa)		
	Uniform inlet velocity	Additional unit of 3.5D upstream	Paraboloidal inlet velocity	Uniform inlet velocity	Additional unit of 3.5D upstream	Paraboloidal inlet velocity
0.58	0.1045	0.0555	0.0502	0.1721	0.2360	0.3038
0.87	0.1745	0.0926	0.0779	0.2942	0.3966	0.5705
1.16	0.2522	0.1349	0.1065	0.4377	0.5743	0.8928
1.46	0.3360	0.1837	0.1366	0.6023	0.7747	1.2759
1.74	0.4249	0.2335	0.1652	0.7878	0.9762	1.6755
2.03	0.5184	0.2890	0.1952	0.9941	1.1980	2.1309
2.32	0.6161	0.3481	0.2252	1.2179	1.4320	2.6272

where the subscript '*geometry*' may be bifurcation, bent or straight depending on whether the straight section follows a bifurcation module, a bent pipe or a straight pipe, and $\Delta p_{0L,\ straight}$ is the loss of total pressure in the straight section following an equivalent straight pipe module. The loss potential is so defined that it is equal to zero for a straight pipe. This allows us to determine the losses incurred in the straight section due to flow division, flow path curvature and cross-sectional shape changes.

Fig. 25 shows the variation with inlet velocity of the loss potential ϕ for three bifurcations (A.R. $=\sqrt[3]{2}$, 1 and $1/\sqrt[3]{2}$) and their equivalent bent pipes (denoted by the same number as the corresponding bifurcation in Table 6). The loss potential is found to increase with V_{inlet} for the bent pipes as well as the bifurcations. Fig. 25 shows that ϕ for all three bifurcations and their equivalent bent pipes are positive in the range of inlet velocities considered here. This quantitatively establishes our qualitative finding from Tables 7 and 8 that $\Delta p_{0L,\ bifurcation}$ and $\Delta p_{0L,\ bent}$ are greater than $\Delta p_{0L,\ straight}$. For any value of A.R. (shown in Fig. 15), $\phi_{bifurcation}$ is always greater than ϕ_{bent} in the range of inlet velocities considered here. This, combined with the fact that $\Delta p_{0,\ bifurcation}$ is smaller than $\Delta p_{0,\ bent}$ (Table 7), indicates that although the loss of total pressure in the bifurcation module alone is smaller than that in the bent pipe alone (i.e. without the following cylindrical sections), the combined effects of flow division, flow path curvature, and cross-sectional shape and area changes in the bifurcation induces greater potential to incur energy losses in the following straight section.

It is also found in Fig. 25 that the difference between the loss potential for the bifurcation and its equivalent bent pipe increases as V_{inlet} increases. This indicates that probably the inertial effects associated with the flow play a major role in inducing greater energy losses in the bifurcation as compared to that in the equivalent bent pipe. Another interesting observation that can be made from the figure is that as A.R. decreases from $\sqrt[3]{2}$ to $1/\sqrt[3]{2}$, the difference between $\phi_{bifurcation}$ and ϕ_{bent} increases.

An increase of inlet diameter and a decrease of area ratio in the bent pipes lead to a reduction in the loss potential

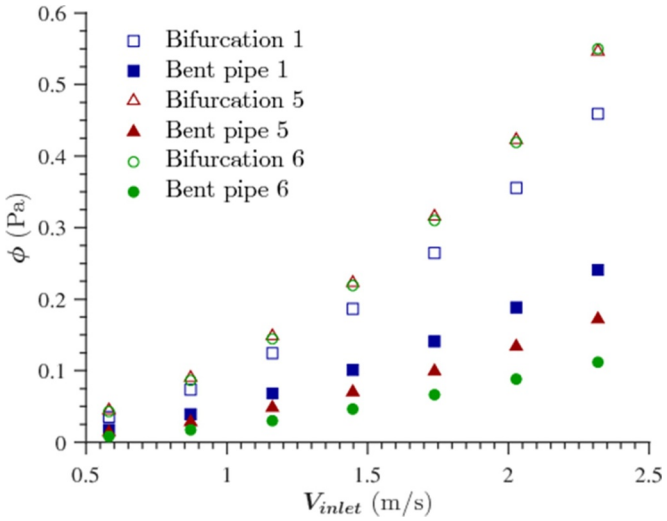

Fig. 25. Variation of the loss potential ϕ with V_{inlet} (uniform distribution) for three 70° bifurcations (with $L_{straight}/D_{daughter}$ = 3.5) and their constituent 35° bent pipes. (Bent pipe *n* refers to the equivalent bent pipe of Bifurcation *n* in Table 6).

($D_{inlet,\ Bent\ pipe\ 1} < D_{inlet,\ Bent\ pipe5}$ and A.R.$_{Bent\ pipe1} >$ A.R.$_{Bent\ pipe5}$ leads to $\phi_{Bent\ pipe,1} > \phi_{Bent\ pipe,\ 5}$). On the other hand, an increase of inlet diameter and a decrease of area ratio in the bifurcations lead to an increase in the loss potential ($D_{inlet,\ Bifurcation1} < D_{inlet,\ Bifurcation5}$ and A.R.$_{Bifurcation1} >$ A.R.$_{Bifurcation5}$). An important observation that can be made from Fig. 25 is that the loss potential for Bifurcations 5 and 6 are nearly the same in the shown range of inlet velocities. For a fixed inlet velocity V_{inlet} (which is used as the x−axis in Fig. 20), an increase of D_{inlet} indicates an increase in the flow rate through the bifurcation. The loss potential for a bifurcation increases with an increase of flow rate. An increase of the area ratio (A.R.) is found to result in an increase in

Table 10
Variation of the loss of total pressure (Δp_0) with flow rate across a bifurcation module (Bifurcation 5:D_{inlet} = 11.23 mm, A.R. = 1) and across a straight section ($L_{straight}/D_{daughter}$ = 3.5) following the bifurcation module for two skewed inlet velocity distributions.

V_{avg}(m/s) at inlet	$\Delta p_{0,\ bifurcation}$ (Pa)		$\Delta p_{0L,\ bifurcation}$ (Pa)			
	Skewed inlet velocity I	Skewed inlet velocity II	Skewed inlet velocity I		Skewed inlet velocity II	
			Left daughter	Right daughter	Left daughter	Right daughter
0.58	0.0773	0.0915	0.2730	0.2010	0.2548	0.1910
0.87	0.1363	0.1751	0.4872	0.3425	0.4924	0.3151
1.16	0.2019	0.2771	0.7367	0.5125	0.7946	0.4791
1.46	0.2723	0.4018	1.0208	0.7178	1.1721	0.7016
1.74	0.3445	0.5344	1.3063	0.9351	1.5854	0.9451
2.03	0.4239	0.6866	1.6201	1.1878	2.0794	1.2288
2.32	0.5057	0.8529	1.9436	1.463	2.6453	1.5444

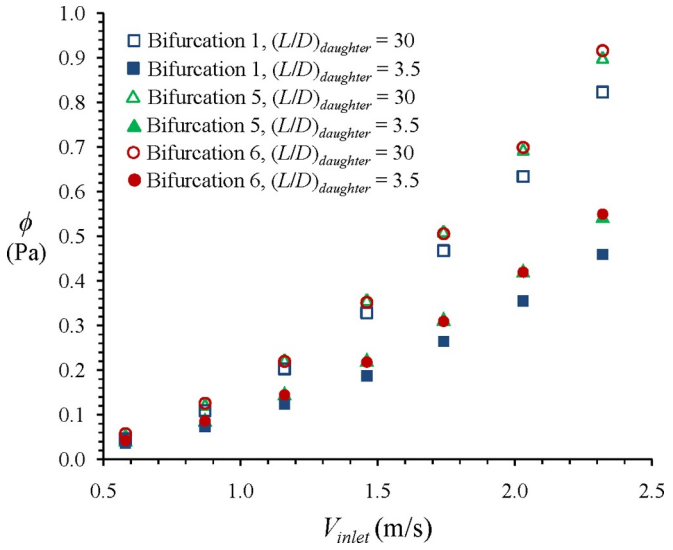

Fig. 26. Variation of the loss potential ϕ with V_{inlet} (uniform velocity distribution) for three bifurcation flow units with the straight length to diameter ratio (L/D) of the daughter branches equal to (a) the practically observed value of 3.5 and, (b) the value required to fully regain the paraboloidal profile (L/D = 30). Here, we refer to $L_{straight}/D_{daughter}$ as $(L/D)_{daughter}$ for ease of representation.

the loss potential due to enhanced asymmetry in the cross-sectional velocity distribution (compare the velocity contours for the bifurcation in Figs. 8–10). The inlet diameter for Bifurcation 5 is 11.23 mm while that for Bifurcation 6 in 12.60 mm. The value of A.R. for Bifurcation 5 is 1.00 whereas that for Bifurcation 6 is 0.79. The combined effect of the above-mentioned relations is that the loss potentials for the two bifurcations turn out to be of nearly the same magnitude.

In Section 5.4, we discussed how the flow field evolves in the straight section following the bifurcation module. It is found that, for uniform inlet velocity and for the range of inlet velocity considered, a length of $L_{straight}/D_{daughter} \sim 30$ is sufficient to obtain paraboloidal velocity in the daughter branch. From the definition of loss potential it may easily be deduced that the loss potential would be maximum ($\phi_{\max}$) for this length ($L_{straight}/D_{daughter} \sim 30$) of the daughter and would remain constant at this value if the length of the straight portion is increased any further. The usually observed length of the daughter branch in natural/biological systems is however $L_{straight}/D_{daughter} = 3.5$ (Pedley et al., 1970a,b, 1971). Fig. 26 shows the loss potential for the usually observed daughter branch length ($L_{straight}/D_{daughter} = 3.5$) and the maximum value ($\phi_{\max}$) obtained when the daughter branch length is taken sufficiently long so that the flow fully recovers. Three bifurcation flow units are considered here (the same as in Fig. 25). It is found that the difference between the two values of ϕ at a given value of V_{inlet} increases as V_{inlet} increases. This may be attributed to the fact that the recovery length increases with V_{inlet}, which results in a greater length of the daughter branch where the loss in the straight section following the bifurcation exceeds that in the straight pipe. However, it is to be remembered that the full recovery length would rarely be present in practical branching networks, and hence the values of $\phi_{\max}$ would seldom assume importance in the estimation of losses in elaborate branching networks. However, the loss potential values for daughter branch lengths of 3.5D may be used along with the Poiseuille loss expression to approximately calculate the loss of total pressure in the straight sections in branching networks.

While the loss potential ϕ for a bifurcation flow unit quantifies the increase in loss of total pressure occurring in the straight section following a bifurcation module as compared to that in a similar straight section following an equivalent straight pipe, it does not give any information regarding the relative importance of that increase when

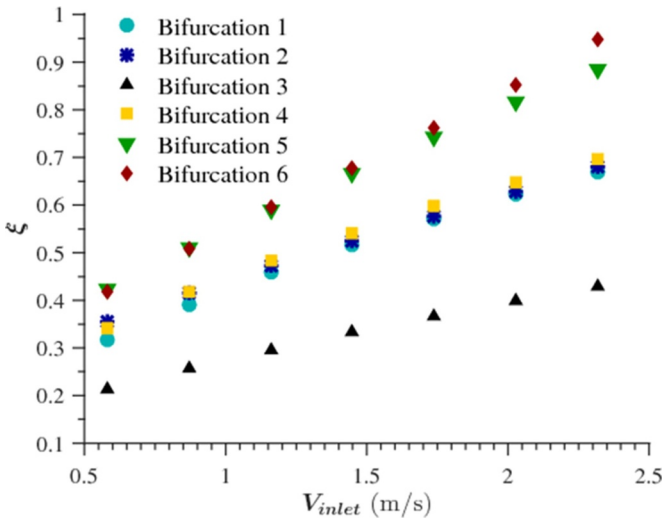

Fig. 27. Variation of the relative loss potential ξ with V_{inlet} (uniform distribution) for 6 different 70° bifurcation geometries (Table 6) with $L_{straight}/D_{daughter}$ = 3.5.

compared to the drop of total pressure across that bifurcation module itself. For this purpose, a relative loss potential ξ is defined as follows:

$$\xi = \frac{\phi_{bifurcation}}{\Delta p_{0,bifurcation}} \tag{10}$$

Here, $\Delta p_{0,\ bifurcation}$ is the loss of total pressure across a given bifurcation module and $\phi_{bifurcation}$ is the loss potential for that bifurcation flow unit. It may be seen in Eq. (10) that the relative loss potential depends on the loss incurred in the bifurcation itself ($\Delta p_{0,\ bifurcation}$) in addition to the inlet diameter and area ratio (on which $\phi_{bifurcation}$ depends).

Fig. 27 shows the variation of the relative loss potential ξ with V_{inlet} for six different bifurcation flow units (refer to Table 6), each with daughter branches of $L_{straight}/D_{daughter} = 3.5$. For a given bifurcation, ξ increases monotonically with V_{inlet}. The loss potential was found to increase with an increase in inlet diameter or area ratio (Fig. 25). Since $D_{inlet,\ Bifurcation\ 1} < D_{inlet,\ Bifurcation2}$ and $\text{A.R.}_{Bifurcation1} > \text{A.R.}_{Bifurcation\ 2}$, $\phi_{bifurcation}$ is almost the same for Bifurcations 1 and 2. Moreover, since $\Delta p_{0,\ bifurcation}$ is almost the same for these two bifurcations, the relative loss potential ($\xi = \phi_{bifurcation}/\Delta p_{0,bifurcation}$) turns out to be nearly equal for Bifurcations 1 and 2. The near-coincidence of the ξ values for Bifurcations 2 and 4 cannot be attributed to such relations because $D_{inlet,\ Bifurcation2} < D_{inlet,\ Bifurcation4}$ and $\text{A.R.}_{Bifurcation2} < \text{A.R.}_{Bifurcation4}$ (which would indicate that $\phi_{Bifurcation2} < \phi_{Bifurcation\ 4}$). The reason for the nearly equal ξ values for Bifurcations 2 and 4 for a given inlet velocity is the lower values of $\Delta p_{0,\ bifurcation}$ for Bifurcation 4 that may be attributed to the shorter length of the flow path ($(L_1 + L_2)/D_{inlet}$) in it.

It is found that, within the ranges of parameters tested, the value of ξ can become of the order 1, which indicates that the additional loss of total pressure in the straight section following the bifurcation, over and above that in a similar straight section following an equivalent straight pipe is of the order of the loss in the bifurcation module itself. Thus, it is inferred from the order of values of ξ that the various geometric factors governing the bifurcation flow induce at the end-plane of the bifurcation module significant potential for additional loss of total pressure in the following straight section. Comparing Tables 7 and 8, and using Eq. (8), it is seen that the loss in total pressure across the bifurcation module itself ($\Delta p_{0,\ bifurcation}$) lies in the range 30–40% of that occurring across the flow unit ($\Delta p_{0t,\ bifurcation}$) consisting of the bifurcation module with straight sections added to its end-planes (Fig. 2). This shows that the assumption made in several previous references that the loss in the bifurcation module itself is negligible was not appropriate.

6. Conclusion

A systematic computational investigation is performed to accurately determine the modifications to a three-dimensional flow field caused by a bifurcation module and to study the downstream evolution of the generated flow field. One uniqueness of the present study is that it does not simply determine the final solution in a complex geometry by the application of CFD as a black-box tool, instead it seeks to attribute the final solution to more elemental aspects of the specified problem thereby enhancing understanding. Thus it is identified how the complex flow solutions arise due to five factors, viz. flow division at the bifurcation ridge, flow path curvature in the bifurcation module, possible change in cross-sectional area from mother to daughter branches, complex shape changes in the bifurcation module and inertia of the flow. This simultaneously provides physical insight into the mechanisms of loss in a bifurcation and its constituent elements. The detailed analysis is systematized here by establishing two novel methods of construction of a bifurcation, viz. “co-joining of two bent pipes” and “splitter in a pipe”, and by formally deriving the equivalence condition for the flow in a bifurcation and its constituent elements. Through this systematization an attempt is made to understand comprehensively the complexity of the fluid dynamics occurring in a single bifurcation, which is often masked in the usual studies of flow in large bifurcating networks. Altogether 14 different bifurcation geometries, a large range of inlet Reynolds number in the laminar regime (400–2000), five different inlet velocity profiles (of which three are axisymmetric and the remaining two consists of skewed primary velocity distribution coupled with secondary motion at the inlet plane), multiple geometries of the downstream branch and about 500 separate three-dimensional computations used in this study provide a degree of generalization that is not available elsewhere.

The fluid dynamic effects of flow division is isolated here by considering the flow in a straight pipe with a splitter plate in the middle (Fig. 12), which may be viewed as a bifurcation with zero bifurcation angle (thus eliminating flow curvature effects) with semi-circular daughters (thus eliminating the effects of change in cross-sectional area and shape). The presence of the splitter plate results in the formation of additional boundary layers on its two sides (or equivalently along the inner edges of the bifurcation in this case), and induces secondary motion that pushes fluid away from it. For a uniform inlet flow, the developed boundary layers on the splitter and the induced secondary motion pushes the location of maximum velocity towards the outer edges of the cross-sections of the daughter branches (this tendency is opposite to that caused by the flow curvature effects described in the next paragraph). The decrease of static (Δp) and total (Δp_0) pressure across the flow unit is significantly increased due to the placement of a splitter plate in a straight pipe (Table 5), indicating that flow division alone results in additional losses in the bifurcation as compared to that in pipe flow.

Flow path curvature is primarily responsible for the development of skewed velocity distributions with the maximum velocity shifted from the center of the cross-section towards the outer edge in the bent pipe (Fig. 7), and, associated Dean-type secondary fluid motion (Fig. 11). The fluid dynamic effects of the curved nature of the flow path in a bifurcation is determined by comparing the flow in a straight pipe with a splitter plate along the middle to that in a bifurcation (70° used here) with semi-circular daughters (thus eliminating the effects of change in cross-sectional area and shape). There is a tendency of setting up a secondary flow due to curvature effects from the outer edges of the bifurcation towards the inner edges along the diameter of the cross-section. This fluid motion forms a part of the Dean-type secondary circulation in the semi-circular daughters of the 70° bifurcation, and is attributable to curvature effects alone (Figs. 12–14). Comparison of the pressure losses (Δp and Δp_0) for a straight pipe and a bent pipe (Table 4), or that for 0° and 70° bifurcations with semi-circular daughters (Table 5) shows that flow path curvature results in an increase in the values of both Δp and Δp_0.

The effects of change of cross-sectional shape alone (i.e. cross-sectional area remaining the same) are exemplified here (Fig. 12 and Table 5) by comparing the flow in a straight pipe having a splitter plate to that in a bifurcation having very small bifurcation angle and circular daughter branches. Both the maximum velocity at a cross-section in the daughter branches and the pressure losses across the flow unit are found to decrease due to the change of cross-sectional shape from semi-circular to circular. However, since the effect of flow path curvature may affect the pressure losses in the opposite sense, there may sometimes be a small increase of Δp and Δp_0 when the change of cross-sectional shape of the daughter branches from semi-circular to circular takes place in the presence of large flow path curvature (compare values of Δp_0 in bifurcations with circular and semi-circular daughters in Table 5).

The fluid dynamic effects of the change of cross-sectional area (keeping the shape same) in a bifurcation are determined here by comparing the flows in 70° bifurcations (with circular daughter branches) with area ratio (A.R.) values of 2, 1 and 2/3. Figs. 8–11 show the effects of area ratio when a bifurcation is constructed by the method of “co-joining of two bent pipes”, and Figs. 12 and 13 show the same when a bifurcation is formed by the method of “splitter in a pipe”. An increase in the value of A.R. results in an increase in the non-uniformity in velocity distribution and a decrease in the average secondary (and primary) velocity at a cross-section in the daughter branches.

The change of cross-sectional shape from circular to oval (Fig. 1) in the initial portion of the bifurcation generates a secondary motion from near the upper and lower walls towards the central axis of the mother branch. As a result of the above-mentioned up-down motion and two opposite sideways motion (from the outer edges of the bifurcation towards the inner edges due to curvature and from the inner edges towards the outer edges due to flow division effects respectively) at a cross-section, a saddle-point type pattern is observed in the secondary motion in the bifurcation module for uniform inlet flow (Fig. 16). [However, such a pattern is not found for a paraboloidal inlet velocity where the curvature effects are stronger due to the non-uniformity in the inlet flow (Fig. 18).]

A comparison of Figs. 16, 18, 20, 21 and 22 shows that the inlet velocity distribution has a significant impact on the flow field in the bifurcation module. As an example, asymmetry in the inlet profile of primary velocity with respect to the bifurcation ridge (as are the cases shown in Figs. 21 and 22) results in unequal flow distribution among the daughter branches (although they are geometrically identical). Similarly it is found that, when a helical motion (i.e. secondary motion along with the primary flow) is prescribed at the inlet (as are the cases shown in Figs. 21 and 22), the anti-Dean type secondary motion may be produced just in a single bifurcation which is usually reported only in a large branching network (Guha and Pradhan, 2017) and did not appear in all other studies of a single bifurcation module where various profiles of primary velocity are prescribed at the inlet without any secondary motion there. The impact of inlet velocity profiles on the pressure loss quantities is summarized in Tables 9 and 10.

The complex physical processes of equilibration through which the flow field created by a bifurcation module relaxes to the paraboloidal velocity profile (if sufficient length is provided in the downstream branches) are graphically illustrated in Figs. 23 and 24. It may appear surprising at first sight that the three-dimensional flow modifications made by a bifurcation module are such that a transformation of paraboloidal at inlet to paraboloidal velocity distribution in a daughter branch takes longer distance than a transformation of uniform to paraboloidal velocity distribution. However, it is unlikely that such recovery lengths (of the order 30–50 times $D_{daughter}$) would be available in a practical (natural or engineered) branching network, and a value of $L_{straight}/D_{daughter} = 3.5$ is adopted here for generic computations, which is found in many natural/biological systems.

Not only the loss is determined across a bifurcation module, that is

directly determinable experimentally or computationally, but the power of CFD is utilized to develop new methods of quantifying the potential for loss generation in subsequent units that follow the bifurcation module under study (quantified here by introducing two new parameters - the loss potential ϕ defined by Eq. (9) and the relative loss potential ξ defined by Eq. (10)). Calculations show that the loss of total pressure (Δp_0) across a bifurcation is smaller than that across the bent pipe itself, for the equivalent flow condition established here (Table 7). A contributory factor to this finding may be visualized by the partial removal of the internal wall in the formation of the bifurcation from the co-joining of two bent pipes. Use of Eq. (8) and the data given in Tables 7 and 8 show consistently that $\Delta p_{0L,\ bifurcation} > \Delta p_{0L,\ bent}$ where Δp_{0L} is the loss of total pressure in the following straight pipe. This provides a new insight in the loss mechanism introduced by the three identified major aspects of a bifurcation module, viz. the flow division at the bifurcation ridge, flow path curvature in the module, and variations of area and shape of the cross-section. Present computations establish that the difference between the loss potentials of a bifurcation and its constituent bent pipes ($\phi_{bifurcation} - \phi_{bent}$) increases with an increase in V_{inlet} and with a decrease in the area ratio (A.R.), being particularly significant when the A.R. goes below 1.

Based on extensive computations for 9 different bifurcations at various flow rates, new correlations are proposed here (see Appendix) for estimating the loss across a bifurcation and the loss across a straight section following a bifurcation as functions of $(L_1 + L_2)/D_{inlet}$, A.R. and Re. From a study of Tables 7–10, it is apparent that the loss depends on many factors. However, a suggestion for a generic methodology also emanates from these extensive computations that, in the absence of three-dimensional computations like the present ones, the use of Eq. (A2) (for uniform inlet flow) for the estimation of loss across a bifurcation module ($\Delta p_{0,\ bifurcation}$) situated in a branching network and the use of Eq. (A5) (for paraboloidal inlet velocity) for the estimation of loss in the straight section following a bifurcation module ($\Delta p_{0L,\ bifurcation}$) may produce approximate but realistic answers in system studies in the Reynolds number range 400–2000 (although no simple loss model can capture the flow asymmetry between the two geometrically similar daughter branches of a bifurcation).

Computed values of ξ for bifurcations indicate that the loss potential may be of the same order of magnitude as the loss of total pressure across the bifurcation itself (Fig. 27). A complementary interpretation can be formed from a comparison of Table 7 and Table 8 that, within the ranges of the parameters tested, the loss in total pressure across just the bifurcation module itself may lie in the range 30–40% of that taking place across a bifurcation flow unit (Fig. 2), showing that the assumption made in several previous references that the loss in the bifurcation module itself is negligible was not appropriate.

Appendix. Correlation for pressure loss in bifurcations

Measured inspiratory velocity profiles in symmetric bifurcation geometries were used by Pedley et al. (1970a,b, 1971) to calculate the viscous dissipation occurring in a daughter branch downstream of a bifurcation. They assumed that all viscous dissipation occurs in the straight section of the daughter branch following a bifurcation, and that no dissipation occurs in the bifurcation itself. They presented their findings through a variable Z which specifies the ratio of the actual energy dissipation in the branch to the Poisseuille dissipation. Mathematically, it takes the following form:

$$Z = \frac{C}{4\sqrt{2}}\left(\mathrm{Re}\frac{d}{L}\right)^{1/2} \tag{A1}$$

Here, d and L are respectively the diameter and length of the daughter branch, Re is the Reynolds number and C is a constant whose value depends on the bifurcation angle and value of A.R. They found that the value of Z downstream of a bifurcation is always greater than unity.

It was found in the course of the present work that the effect of bifurcation angle on the value of Δp_0 is small. Accordingly, we have concentrated our efforts on a particular value of θ, viz. $\theta = 70°$. Based on extensive computations covering nine different bifurcations (Table 6) and seven values of inlet Reynolds number Re for each bifurcation, a correlation is developed to determine the loss of total pressure for flow of air across a bifurcation module in the range $400 \le \mathrm{Re} \le 2000$ for a uniform inlet velocity distribution:

$$\frac{\Delta p_{0,bifurcation}}{\rho V_{inlet}^2} = 15.97\left(\frac{L_1 + L_2}{D_{inlet}}\right)(\mathrm{A.R.})^{-0.7}\mathrm{Re}^{-0.7} \tag{A2}$$

In Eq. (A2), D_{inlet} refers to the diameter at the inlet to the bifurcation module and L_1 and L_2 refer to the centreline lengths of the portions of the mother and daughter branches respectively which form the bifurcation module (Fig. 2). A.R. refers to the ratio of the total cross-sectional area at the outlet (i.e. sum of the area of flow in the two daughters) to the cross-sectional area at the inlet of the bifurcation. Eq. (A2) is able to predict the value of $\Delta p_{0,\ bifurcation}$ to within $\pm$ 8% of the CFD results.

We also performed computations for the flow of air in the above-mentioned nine bifurcations when they are followed by straight sections (Fig. 2) such that $L_{straight}/D_{daughter} = 3.5$ (Pedley et al., 1970a,b, 1971). The loss of total pressure across the straight section following the bifurcation module in the range $400 \le \mathrm{Re} \le 2000$ for a uniform velocity distribution at the inlet to the bifurcation may be determined by the following expression:

$$\frac{\Delta p_{0L,bifurcation}}{\rho V_{inlet}^2} = 16.85\left(\frac{L_1 + L_2}{D_{inlet}}\right)^{-0.7}(\mathrm{A.R.})^{-1.3}\mathrm{Re}^{-0.6} \tag{A3}$$

The loss of total pressure determined by Eq. (A3) is found to lie within $\pm$ 10% of the CFD results. The loss of total pressure across a "flow unit" comprising a bifurcation module and following straight sections can be approximately ascertained by summing the energy losses given by Eqs. (A2) and (A3).

Similarly, the loss of total pressure for flow of air across a bifurcation module in the range $400 \le \mathrm{Re} \le 2000$ for a paraboloidal inlet velocity distribution may be predicted from the following expression:

$$\frac{\Delta p_{0,bifurcation}}{\rho V_{inlet}^2} = 23.91c_1\left(\frac{L_1 + L_2}{D_{inlet}}\right)(\mathrm{A.R.})^{-1}\mathrm{Re}^{-c_2} \tag{A4}$$

where$c_1 = 1$, $c_2 = 0.9$ forA.R. ≥ 1, and $c_1 = 0.5$, $c_2 = 0.75$ forA.R. < 1. The loss of total pressure across the straight section ($L_{straight}/D_{daughter} = 3.5$) following the bifurcation module in the range $400 \le \mathrm{Re} \le 2000$ for a paraboloidal inlet velocity distribution may be predicted by the following expression:

$$\frac{\Delta p_{0L,bifurcation}}{\rho V_{inlet}^2} = 12.52\left(\frac{L_1 + L_2}{D_{inlet}}\right)^{-0.07}(\text{A.R.})^{-0.25}\text{Re}^{-0.46} \quad \text{(A5)}$$

The loss of total pressure determined by Eqs. (A4) and (A5) are found to lie within ± 10% of the CFD results.

References

ANSYS Academic Research, Release 15.0, 2014, ANSYS, Inc. Canonsburg, USA.

Banko, A.J., Coletti, F., Schiavazzi, D., Elkins, C.J., Eaton, J.K., 2015. Three-dimensional inspiratory flow in the upper and central human airways. Exp. Fluids 56 (6), 1–12.

Barth, T.J., Jespersen, D.C., 1989. The design and application of upwind schemes on unstructured meshes, In AIAA 27th Aerospace Sciences Meeting, Reno, Nevada, pp. 366.

Bauer, K., Nof, E., Sznitman, J., 2017. Revisiting high-frequency oscillatory ventilation in vitro and in silico in neonatal conductive airways. Clin. Biomech. 66, 50–59.

Berger, S.A., Talbot, L., Yao, L.S., 1983. Flow in curved pipes. Annu. Rev. Fluid Mech. 15 (1), 461–512.

Blyth, M.G., Mestel, A.J., 1999. Steady flow in a dividing pipe. J. Fluid Mech. 401, 339–364.

Celik, I.B., Ghia, U., Roache, P.J., 2008. Procedure for estimation and reporting of uncertainty due to discretization in CFD applications. Trans. ASME, J. Fluids Eng. 130 (7), 078001:1–4.

Chang, H.K., El Masry, O.A., 1982. A model study of flow dynamics in human central airways. Part I: Axial velocity profiles. Respir. Physiol. 49 (1), 75–95.

Comer, J.K., Kleinstreuer, C., Zhang, Z., 2001. Flow structures and particle deposition patterns in double-bifurcation airway models. Part 1. Air flow fields. J. Fluid Mech. 435, 25–54.

Das, P., Nof, E., Amirav, I., Kassinos, S.C., Sznitman, J., 2018. Targeting inhaled aerosol delivery to upper airways in children: insight from computational fluid dynamics (CFD). PLoS ONE 13 (11), 0207711.

Fresconi, F.E., Prasad, A.K., 2007. Secondary velocity fields in the conducting airways of the human lung. Trans. ASME, J. Biomech. Eng. 129 (5), 722–732.

Guha, A., 1994. Thermal choking due to nonequilibrium condensation. Trans. ASME, J. Fluids Eng. 116 (3), 599–604.

Guha, A., 2008. Transport and deposition of particles in turbulent and laminar flow. Annu. Rev. Fluid Mech. 40, 311–341.

Guha, A., Pradhan, K., 2017. Secondary motion in three-dimensional branching networks. Phys. Fluids 29 (6), 063602 1-24.

Guha, A., Young, J.B., 1991. Time-marching prediction of unsteady condensation phenomena due to supercritical heat addition. In Turbomachinery: Latest Developments in a Changing Scene. Institution of Mechanical Engineers, London, UK, pp. 167–177 ISBN 0852987617.

Guha, A., Pradhan, K., Halder, P.K., 2016. Finding order in complexity: A study of the fluid dynamics in a three-dimensional branching network. Phys. Fluids 28 (12), 123602 1-32.

Horlock, J.H., 1956. Some experiments on the secondary flow in pipe bends. Proc. R. Soc. London, Ser. A 234, 335–346.

Jeong, J., Hussain, F., 1995. On the identification of a vortex. J. Fluid Mech. 285, 69–94.

Kang, M.Y., Hwang, J., Lee, J.W., 2011. Effect of geometric variations on pressure loss for a model bifurcation of the human lung airway. J. Biomech. 44 (6), 1196–1199.

Kitaoka, H., Takaki, R., Suki, B., 1999. A three-dimensional model of the human airway tree. J. Appl. Physiol. 87 (6), 2207–2217.

Kleinstreuer, C., Zhang, Z., 2009. An adjustable triple-bifurcation unit model for air-particle flow simulations in human tracheobronchial airways. Trans. ASME, J. Biomech. Eng. 131 (2), 021007.

Koullapis, P.G., Kassinos, S.C., Bivolarova, M.P., Melikov, A.K., 2016. Particle deposition in a realistic geometry of the human conducting airways: Effects of inlet velocity profile, inhalation flowrate and electrostatic charge. J. Biomech. 49 (11), 2201–2212.

Liu, Y., So, R.M.C., Zhang, C.H., 2002. Modeling the bifurcating flow in a human lung airway. J. Biomech. 35 (4), 465–473.

Longest, P.W., Vinchurkar, S., 2007. Effects of mesh style and grid convergence on particle deposition in bifurcating airway models with comparisons to experimental data. Med. Eng. Phys. 29 (3), 350–366.

Luo, H.Y., Liu, Y., 2008. Modeling the bifurcating flow in a CT-scanned human lung airway. J. Biomech. 41 (12), 2681–2688.

Massey, B.S., Ward-Smith, J., 1998. Mechanics of Fluids, 8th edition. Taylor & Francis, New York, USA.

Mei, Y., Guha, A., 2005. Implicit numerical simulation of transonic flow through turbine cascades on unstructured grids. Proc. Inst. Mech. Eng. Part A, J. Power Energy 219 (1), 35–47.

Murray, C.D., 1926. The physiological principle of minimum work I. The vascular system and the cost of blood volume. Proc. Natl. Acad. Sci. 12 (3), 207–214.

Murray, J.J., Guha, A., Bond, A., 1997. Overview of the development of heat exchangers for use in air-breathing propulsion pre-coolers. Acta Astronaut. 41 (11), 723–729.

Nowak, N., Kakade, P.P., Annapragada, A.V., 2003. Computational fluid dynamics simulation of airflow and aerosol deposition in human lungs. Ann. Biomed. Eng. 31 (4), 374–390.

Pedley, T.J., 1977. Pulmonary fluid dynamics. Annu. Rev. Fluid Mech. 9 (1), 229–274.

Pedley, T.J., Schroter, R.C., Sudlow, M.F., 1970a. Energy losses and pressure drop in models of human airways. Respir. Physiol. 9 (3), 371–386.

Pedley, T.J., Schroter, R.C., Sudlow, M.F., 1970b. The prediction of pressure drop and variation of resistance within the human bronchial airways. Respir. Physiol. 9 (3), 387–405.

Pedley, T.J., Schroter, R.C., Sudlow, M.F., 1971. Flow and pressure drop in systems of repeatedly branching tubes. J. Fluid Mech. 46 (2), 365–383.

Pourmehran, O., Gorji, T.B., Gorji-Bandpy, M., 2016. Magnetic drug targeting through a realistic model of human tracheobronchial airways using computational fluid and particle dynamics. Biomech. Model. Mechanobiol. 15 (5), 1355–1374.

Pradhan, K., Guha, A., 2019. Fluid dynamics of oscillatory flow in three-dimensional branching networks. Phys. Fluids 31 (6), 063601 1-29.

Roache, P.J., 1997. Quantification of uncertainty in computational fluid dynamics. Annu. Rev. Fluid Mech. 29 (1), 123–160.

Schroter, R.C., Sudlow, M.F., 1969. Flow patterns in models of the human bronchial airways. Respir. Physiol. 7 (3), 341–355.

Singh, M.P., 1974. Entry flow in a curved pipe. J. Fluid Mech. 65 (3), 517–539.

Smith, F.T., 1970. Pipeflows distorted by non-symmetric indentation or branching. Mathematika 23 (1), 62–83.

Smith, F.T., 1976. On entry-flow effects in bifurcating, blocked or constricted tubes. J. Fluid Mech. 78 (4), 709–736.

Smith, F.T., 1977a. Upstream interactions in channel flows. J. Fluid Mech. 79 (4), 631–655.

Smith, F.T., 1977b. Steady motion through a branching tube. Proc. R. Soc. London, Ser. A 355, 167–187.

SolidWorks Release2010, Dassault Systèmes SolidWorks Corporation. Waltham, USA.

Stylianou, F.S., Sznitman, J., Kassinos, S.C., 2016. Direct numerical simulation of particle laden flow in a human airway bifurcation model. Int. J. Heat Fluid Flow 61, 677–710.

Tadjfar, M., Smith, F.T., 2004. Direct simulations and modelling of basic three-dimensional bifurcating tube flows. J. Fluid Mech. 519, 1–32.

Weibel, E.R., 1963. Morphometry of the Human Lung. Springer, Berlin Heidelberg.

Wells, A.K., Jones, I.P., Hamill, S., Bordas, R., 2017. The prediction of viscous losses and pressure drop in models of the human airways. Int. J. Numer. Method. Biomed. Eng. e2898. https://doi.org/10.1002/cnm.2898.

Wilquem, F., Degrez, G., 1997. Numerical modeling of steady inspiratory airflow through a three-generation model of the human central airways. Trans. ASME, J. Biomech. Eng. 119 (1), 59–65.

Yung, C.N., De Witt, K.J., Keith Jr, T.G., 1990. Three-dimensional steady flow through a bifurcation. Trans. ASME, J. Biomech. Eng. 112 (2), 189–197.

Zhang, Z., Kleinstreuer, C., Kim, C.S., 2001. Flow structure and particle transport in a triple bifurcation airway model. Trans. ASME, J. Fluids Eng. 123 (2), 320–330.

Zhao, Y., Lieber, B.B., 1994a. Steady inspiratory flow in a model symmetric bifurcation. Trans. ASME, J. Biomech. Eng. 116 (4), 488–496.

Zhao, Y., Lieber, B.B., 1994b. Steady expiratory flow in a model symmetric bifurcation. Trans. ASME, J. Biomech. Eng. 116 (3), 318.

Zhao, Y., Brunskill, C.T., Lieber, B.B., 1997. Inspiratory and expiratory steady flow analysis in a model symmetrically bifurcating airway. Trans. ASME, J. Biomech. Eng. 119 (1), 52–58.